The Journal of Physiology

Piezo1 stretch-activated channel activity differs between murine bone marrow-derived and cardiac tissue-resident macrophages

Ana Simon-Chica[1,2,*], Alexander Klesen[1,3,*], Ramona Emig[1,4], Andy Chan[5], Joachim Greiner[1,4], Dominic Grün[5], Achim Lother[6,7], Ingo Hilgendorf[8], Eva A. Rog-Zielinska[1], Ursula Ravens[1], Peter Kohl[1,4], Franziska Schneider-Warme[1,4] and Rémi Peyronnet[1]

[1] *Institute for Experimental Cardiovascular Medicine, University Heart Center Freiburg – Bad Krozingen, Medical Center – University of Freiburg and Faculty of Medicine, University of Freiburg, Freiburg, Germany*
[2] *Centro Nacional de Investigaciones Cardiovasculares Carlos III, Madrid, Spain*
[3] *Department of Congenital Heart Defects and Paediatric Cardiology, University Heart Center Freiburg – Bad Krozingen, Medical Center – University of Freiburg and Faculty of Medicine, University of Freiburg, Freiburg, Germany*
[4] *Centre for Integrative Biological Signalling Studies (CIBSS), Faculty of Biology, University of Freiburg, Freiburg, Germany*
[5] *Würzburg Institute of Systems Immunology, Max Planck Research Group at Julius-Maximilians-University Würzburg, Würzburg, Germany*
[6] *Interdisciplinary Medical Intensive Care, Medical Center – University of Freiburg and Faculty of Medicine, University of Freiburg, Freiburg, Germany*
[7] *Institute of Experimental and Clinical Pharmacology and Toxicology, Faculty of Medicine, University of Freiburg, Freiburg, Germany*
[8] *Department of Cardiology and Angiology, University Heart Center Freiburg – Bad Krozingen, Medical Center – University of Freiburg and Faculty of Medicine, University of Freiburg, Freiburg, Germany*

Handling Editors: Natalia Trayanova & Eilidh MacDonald

The peer review history is available in the Supporting Information section of this article (https://doi.org/10.1113/JP284805#support-information-section).

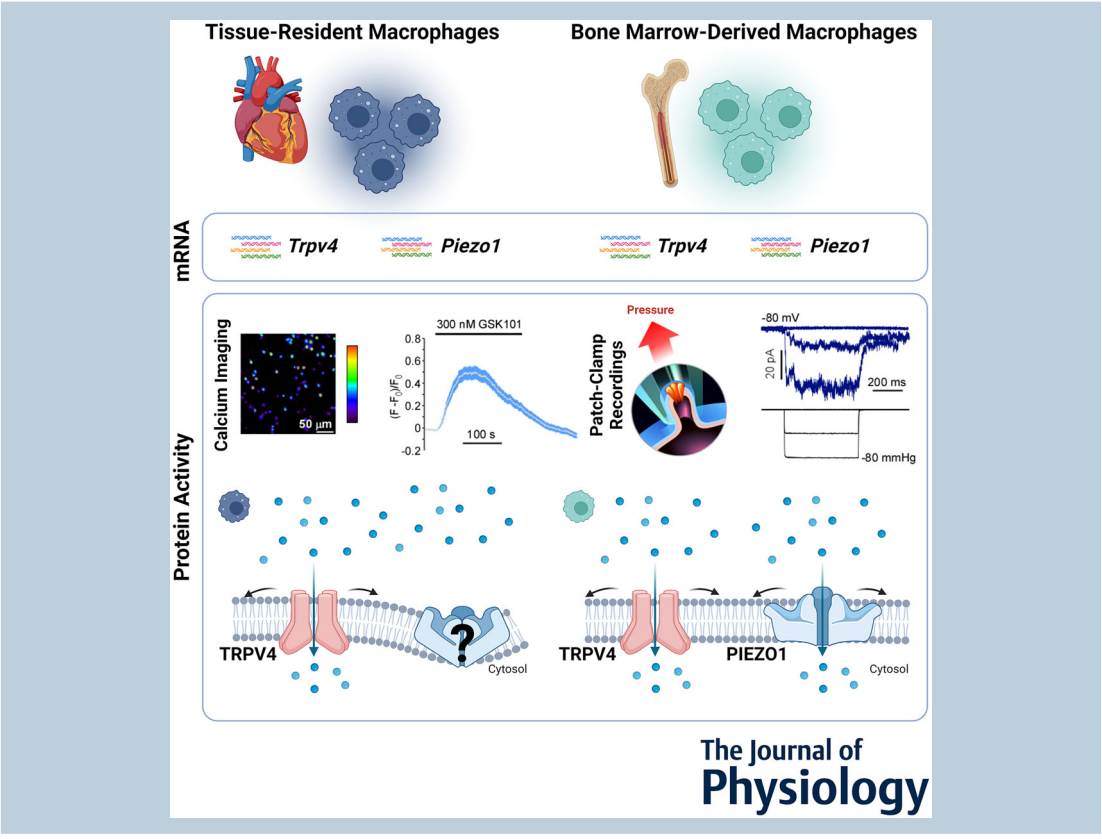

[*] A. Simon-Chica and A. Klesen are co-first authors.

DOI: 10.1113/JP284805

Abstract Macrophages (MΦ) play pivotal roles in tissue homeostasis and repair. Their mechanical environment has been identified as a key modulator of various cell functions, and MΦ mechanosensitivity is likely to be critical – in particular in a rhythmically contracting organ such as the heart. Cultured MΦ, differentiated *in vitro* from bone marrow ($M\Phi_{BM}$), form a popular research model. This study explores the activity of mechanosensitive ion channels (MSC) in murine $M\Phi_{BM}$ and compares it to MSC activity in MΦ enzymatically isolated from cardiac tissue (tissue-resident MΦ; $M\Phi_{TR}$). We show that $M\Phi_{BM}$ and $M\Phi_{TR}$ have stretch-induced currents, indicating the presence of functional MSC in their plasma membrane. The current profiles in $M\Phi_{BM}$ and in $M\Phi_{TR}$ show characteristics of cation non-selective MSC such as Piezo1 or transient receptor potential channels. While Piezo1 ion channel activity is detectable in the plasma membrane of $M\Phi_{BM}$ using the patch-clamp technique, or by measuring cytosolic calcium concentration upon perfusion with the Piezo1 channel agonist Yoda1, no Piezo1 channel activity was observed in $M\Phi_{TR}$. The selective transient receptor potential vanilloid 4 (TRPV4) channel agonist GSK1016790A induces calcium entry in $M\Phi_{TR}$ and in $M\Phi_{BM}$. In MΦ isolated from left-ventricular scar tissue 28 days after cryoablation, stretch-induced current characteristics are not significantly different compared to non-injured control tissue, even though scarred ventricular tissue is expected to be mechanically remodelled and to contain an altered composition of pre-existing cardiac and circulation-recruited MΦ. Our data suggest that the *in vitro* differentiation protocols used to obtain $M\Phi_{BM}$ generate cells that differ from MΦ recruited from the circulation during tissue repair *in vivo*. Further investigations are needed to explore MSC identity in lineage-traced MΦ in scar tissue, and to compare mechanosensitivity of circulating monocytes with that of $M\Phi_{BM}$.

(Received 6 April 2023; accepted after revision 14 March 2024; first published online 11 April 2024)
Corresponding authors R. Peyronnet and F. Schneider-Warme: Institute for Experimental Cardiovascular Medicine, University Heart Center Freiburg – Bad Krozingen, Medical Center – University of Freiburg and Faculty of Medicine, University of Freiburg, Elsässer Straße 2Q, D-79110 Freiburg, Germany. Emails: remi.peyronnet@uniklinik-freiburg.de and franziska.schneider.uhz@uniklinik-freiburg.de

Abstract figure legend Comparative analysis of mechanosensitive ion channels in mouse tissue-resident and bone marrow-derived macrophages. mRNA coding for the mechanosensitive ion channels Piezo1 and TRPV4 is found in both types of macrophages. Piezo1 activity is observed in the plasma membrane of bone marrow-derived macrophages, but not in the membrane of macrophages isolated from heart tissue while TRPV4 activity is found across the macrophage types studied.

Key points

- Bone marrow-derived ($M\Phi_{BM}$) and tissue resident ($M\Phi_{TR}$) macrophages have stretch-induced currents, indicating expression of functional mechanosensitive channels (MSC) in their plasma membrane.
- Stretch-activated current profiles show characteristics of cation non-selective MSC; and mRNA coding for MSC, including Piezo1 and TRPV4, is expressed in murine $M\Phi_{BM}$ and in $M\Phi_{TR}$.
- Calcium entry upon pharmacological activation of TRPV4 confirms functionality of the channel in $M\Phi_{TR}$ and in $M\Phi_{BM}$.
- Piezo1 ion channel activity is detected in the plasma membrane of $M\Phi_{BM}$ but not in $M\Phi_{TR}$, suggesting that $M\Phi_{BM}$ may not be a good model to study the mechanotransduction of $M\Phi_{TR}$.
- Stretch-induced currents, Piezo1 mRNA expression and response to pharmacological activation are not significantly changed in cardiac MΦ 28 days after cryoinjury compared to sham operated mice.

Introduction

Biophysical signals are omnipresent across biological processes. Among them, mechanical stimuli are known to regulate essential cell functions such as migration, differentiation and metabolism (Emig, Zgierski-Johnston et al., 2021; Romani, Valcarcel-Jimenez et al., 2021).

Virtually all cell types are mechanosensitive, i.e. they can sense and respond to mechanical stimuli. MΦ form a heterogeneous cell population with important roles in tissue homeostasis and mediation of inflammatory responses. In many organs, including the heart, MΦ can be divided into (i) tissue-resident ($MΦ_{TR}$), derived from embryonically established components of the myocardium, and (ii) MΦ recruited to the tissue from the blood (monocyte-derived MΦ: $MΦ_{MD}$). In addition, experimental research has relied on MΦ derived *in vitro* from bone marrow ($MΦ_{BM}$) by subjecting the cells to pre-conditioned medium (more detail below) (Weischenfeldt & Porse, 2008). The various MΦ subtypes are characterised by distinct transcriptional profiles, protein expression patterns and functions (Bajpai, Schneider et al., 2018; Chakarov, Lim et al., 2019; Heidt, Courties et al., 2014).

Recent studies have highlighted not only that MΦ communicate with other cells via autocrine and paracrine signalling pathways, but also that they can sense, transmit and respond to electrical (Hulsmans, Clauss et al., 2017; Simon-Chica, Fernández et al., 2022) and mechanical signals (Lee, Du et al., 2022). Several MΦ functions are governed by ion channels (Scheraga, Abraham et al., 2016; Vicente, Escalada et al., 2003; Villalonga, David et al., 2010), including mechanosensitive ion channels (MSC), a family of well-characterised mechanosensors. More specifically, the cation non-selective MSC Piezo1, which is ubiquitously expressed in cells across different species and is involved in a large range of biological processes (Beech & Kalli 2019; Delmas, Parpaite & Coste 2022), has been shown to contribute to the regulation of immune cell activity. In murine $MΦ_{BM}$, genetic deletion of Piezo1 reduces inflammation and promotes wound healing (Atcha, Jairaman et al., 2021). In addition, Piezo1-mediated Ca^{2+} entry is essential for $MΦ_{BM}$ stiffness sensing and modulation of MΦ polarisation (Atcha, Jairaman et al., 2021). Using implantable hydrogels mimicking the stiffness of fibrin clots, Forget, Gianni-Barrera et al. (2019) showed that stiffness-dependent recruitment of circulating monocytes into murine skeletal muscle *in vivo* requires Piezo1. Piezo1 was also found to be involved in shear stress-induced monocyte activation, altering monocyte activity and contributing to valve inflammation (Baratchi, Zaldivia et al., 2020). Recent evidence hints at a regulatory role of Piezo1 in the initiation and progression of chronic inflammation in myocardial fibrosis, atherosclerosis, pulmonary fibrosis, obesity and diabetes (Liu et al., 2022). Solis, Bielecki et al. (2019) further demonstrated that cyclic hydrostatic pressure changes can induce a pro-inflammatory gene expression profile in mouse monocytes via Piezo1, whereas mice lacking Piezo1 in myeloid cells show reduced pulmonary inflammation during bacterial infections or fibrotic autoinflammation.

These findings highlight that Piezo1 expression and/or activity can modulate essential functions of $MΦ_{BM}$ and monocytes. However, there is limited knowledge about the mechanism underlying responses to mechanical stimulation of tissue-resident immune cells. This is of particular interest for $MΦ_{TR}$ that are embedded in mechanically active tissue, such as the rhythmically contracting heart, in which MΦ are exposed to a wide range of mechanical stimuli, including stretch, compression, shear, torsion and bending. Insight into the mechanosensitivity of $MΦ_{TR}$ is a prerequisite for a comprehensive understanding of their role in the maintenance of cardiac structure and function (Hulsmans, Clauss et al., 2017; Nicolas-Avila, Lechuga-Vieco et al., 2020).

Here, we assess MSC expression and activity in murine cardiac $MΦ_{BM}$ and $MΦ_{TR}$. RNA sequencing reveals expression of mRNA coding for several MSC, including Piezo1 and TRPV4, in $MΦ_{BM}$ and $MΦ_{TR}$. Using the patch-clamp technique, we observe stretch-induced currents in isolated $MΦ_{BM}$ and $MΦ_{TR}$ compatible with the activity of cation non-selective MSC. Based on electrophysiological measurements, Ca^{2+} imaging and pharmacological interventions, we suggest that – in contrast to $MΦ_{BM}$ – the contribution of Piezo1 to stretch-activated currents in $MΦ_{TR}$ is minor. This indicates that different molecular mechanisms underlie mechanosensitivity of tissue-resident and *in vitro*-differentiated MΦ.

Ana Simon-Chica studied Biomedical Engineering at the University Carlos III of Madrid, Spain. In 2017 she joined the Institute for Experimental Cardiovascular Medicine (IEKM) in Freiburg, Germany, as a scientific assistant, while also completing a Master's degree in Biomedical Engineering. She performed her PhD studies at the Spanish National Centre for Cardiovascular Research (CNIC) in Madrid, focusing on the role of non-myocytes in cardiac conduction and atrial fibrillation maintenance. She completed her PhD in 2024. **Alexander Klesen** studied human medicine at the University of Freiburg. He obtained his 'Dr med.' degree in 2020 and his medical approbation in 2021. In addition to his clinical duties at the Department for Congenital Heart Defects and Paediatric Cardiology of the University Clinics Freiburg, he works as a Clinician Scientist at IEKM.

Methods

Ethical approval and animal experiments

All animal experiments were carried out according to the guidelines in Directive 2010/63/EU of the European Parliament on the protection of animals used for scientific purposes; they were approved by the local authorities in Baden–Württemberg, Germany (Regierungspräsidium Freiburg, G20/01), and by the animal welfare officer of the Centre for Experimental Models and Transgenic Services-Freiburg (X19/01R).

$M\Phi_{TR}$ were isolated from B6.129P2(Cg)-Cx_3cr_1 $^{tm2.1(cre/ERT2)Litt}$/WganJ mice ($Cx_3cr_1^{eYFP/+}$; JAX stock no. 021160) wherein enhanced yellow fluorescent protein (eYFP) is expressed under the control of the fractalkine Cx_3cr_1 promoter, labelling mononuclear phagocytes, i.e. MΦ, monocytes and dendritic cells (Parkhurst et al., 2013). Mice of both sexes were 8–18 weeks old when used, and litter mates not expressing eYFP served as controls. Murine $M\Phi_{BM}$ were obtained from WT mice of same background (C57BL/6J) as described below. Porcine $M\Phi_{BM}$ were harvested *post mortem* from tibiae of Landrace pigs ($N = 2$), obtained from the slaughter house.

Ventricular cryoablation

Left ventricular cryoinjury and sham surgery were applied to 12-week-old $Cx_3cr_1^{eYFP/+}$ mice. To this end, mice were anaesthetised by intraperitoneal injection of 80–100 µL of anaesthesia solution (20 mg/mL ketamine (Ketaset; Zoetis, Parsippany-Troy Hills, NJ, USA), 1.4 mg/mL xylacin hydrochloride (0.12% Rompun; Bayer, Leverkusen, Germany), in 114 mM NaCl (0.67% m/v; B. Braun Melsungen, Melsungen, Germany)). After induction of deep anaesthesia, eye ointment (Bepanthen containing 50 mg/mL dexpanthenol; Bayer) was applied, 500 µL glucose solution (278 mM glucose = 5% (m/v); B. Braun Melsungen) was injected intraperitoneally, and 250 µL of analgesia solution (10 µg/mL buprenorphine (Temgesic; Indivior Inc., North Chesterfield, VA, USA) in 154 mM NaCl (0.9% m/v, B. Braun Melsungen)) was injected subcutaneously in the neck. Mice were shaved at the left side of the thorax (precordial region) and on the right leg. Mice were placed on a warming platform of a small animal physiology monitoring system (Harvard Apparatus, Holliston, MA, USA), and the front extremities were fixed with tape. A rectal thermometer was inserted to allow regulation of the heating platform to ensure a body temperature of 37°C. Thermometer and tail were fixed with tape. Mice were intubated for positive pressure ventilation (Kent Scientific, Torrington, CT, USA; 40% O_2, 120 breathing cycles per minute). Isoflurane was applied at 5% until the animal stopped spontaneous respiratory movements, and then reduced to 2.0–2.5%. An infrared blood oximeter was attached to the right leg to track haemoglobin oxygen saturation, which was used to adjust the ventilation if needed. The surgical field was disinfected using Softasept N (B. Braun Melsungen). Skin and muscles were cut along the third intercostal space, and a rib spreader was introduced. The pericardium was cut and the epicardial surface dry-blotted using a cellulose pad. A metal probe (stainless steel, 2.5 mm (edge-normal distance) hexagon) pre-chilled in liquid nitrogen was applied for 8–10 s on the free left-ventricular mid-wall, positioned to avoid major coronary vessels. After retraction of the probe, the time until the tissue regained deep-red colour was protocolled (consistently within 5–10 s). For sham surgery, application of the metal probe was skipped. The rib spreader was removed and the thorax closed using a 6-0 silk suture around the third and fourth ribs (4–5 single knots). Before final closure, any remaining air was removed from the thorax using a small cannula. Isoflurane application was stopped and the skin was closed with a 6-0 silk suture. Once the mouse started breathing spontaneously, intubation and fixation were terminated, and the mouse was transferred to a heated and oxygenated wake-up chamber. Analgesia was maintained for 72 h post-ablation by twice-daily subcutaneous injection of 250 µl of buprenorphine (10 µg/mL in 154 mM NaCl; morning and late afternoon). During the night, buprenorphine was supplied via the drinking water (10 µg/mL buprenorphine (Subutex lingual tablets, Indivior) in 20 mM glucose solution). Terminal experiments were performed 21–28 days after ventricular cryoinjury or sham surgery. For single-cell RNA sequencing (scRNA-seq), hearts were harvested on day 1 and day 28 after surgical interventions.

MΦ isolation from murine hearts

$M\Phi_{TR}$ were isolated from murine hearts as previously described (Fernandez, Kopton et al., 2021; Simon-Chica, Fernández et al., 2022). In short, mice were euthanised by cervical dislocation, and hearts were swiftly excised and gently washed with 20 mL of cold phosphate buffered saline (PBS, in mM: NaCl 137, KCl 2.7, Na_2HPO_4 10, KH_2PO_4 1.8). Thereafter, tissue was minced into small pieces and enzymatically digested for 40 min under gentle agitation with a mixture of 450 U/mL collagenase I, 125 U/mL collagenase XI, 60 U/mL DNase I and 60 U/mL hyaluronidase (all Sigma-Aldrich, Munich, Germany) in 1 mL PBS at 37°C. Cells were re-suspended in fluorescence-activated cell sorting (FACS) buffer (PBS with 1% fetal bovine serum (FBS) + 0.1% BSA; all Sigma-Aldrich).

Cardiac $M\Phi_{TR}$ were FACS-purified based on cytosolic eYFP fluorescence using an Aria III cell sorter (BD Biosciences, San Jose, CA, USA). The gating strategy was

based on (1) forward scatter and side scatter signals to eliminate cell debris, (2) side scatter area and side scatter height for doublet discrimination, and (3) eYFP intensity for purification of our cell population of interest. Cells from eYFP-negative littermates served as controls for determining background fluorescence. FlowJo software (BD Biosciences) was used to analyse the FACS data.

Cell culture

FACS-purified $M\Phi_{TR}$ were seeded onto 15-mm uncoated glass coverslips in 24-well plates at a density of 20,000 cells/mL in 1 mL Dulbecco's modified Eagle's medium (DMEM, Thermo Fisher Scientific, Waltham, MA, USA) supplemented with 10% heat-inactivated FBS and 1% penicillin/streptomycin (172 μM streptomycin and 200 μM penicillin, all Sigma-Aldrich) and kept in an incubator for cell culture (5% CO_2, 37°C). Non-adherent cells were removed by changing the medium before functional experiments. Experiments were conducted 5–30 h after cell isolation.

Murine $M\Phi_{BM}$ were differentiated *in vitro* from bone marrow, harvested from murine femurs and tibiae. Epiphyses were removed and a 23G needle was inserted into one end. The bone marrow was flushed by injecting 2–3 mL of PBS per bone. Afterwards, cells were centrifuged (400 *g* for 5 min at 4°C) and cultured for 7 days in DMEM supplemented with 10% FBS, 20% L929-conditioned medium, 5% horse serum (Thermo Fisher Scientific) and 1% penicillin/streptomycin. L929-cell conditioned medium was obtained from the supernatant of L929 cells, which served as a source of recombinant MΦ colony stimulating factor. Preparation of L929-conditioned medium followed the protocol described in (Weischenfeldt & Porse, 2008). Briefly, 0.5×10^6 L929 cells were plated in a 75-cm^2 flask containing 55 mL of L929 medium (DMEM supplemented with 10% heat inactivated FBS and 1% penicillin/streptomycin) and maintained in an incubator containing 5% CO_2 at 37°C. After 7 days, the supernatant was collected, filtered through a 0.22 μm syringe filter (Thermo Fisher Scientific), and used for preparation of $M\Phi_{BM}$ medium. Surplus supernatant not utilised immediately was stored at −20°C. After 7 days in culture, $M\Phi_{BM}$ were harvested using trypsin (Thermo Fisher Scientific) and seeded onto uncoated glass coverslips (same culture conditions as before). Experiments were conducted within 5–30 h after plating the cells.

Porcine $M\Phi_{BM}$ were obtained from tibiae collected from the slaughterhouse and processed within 3 h from sacrifice. Epiphyses were removed, and bone marrow was harvested using a lab spoon and transferred into 10 mL of PBS. Cell suspensions were filtered through a mesh (pore size of 1 mm^2) and red blood cells were lysed with red blood cell lysis buffer (Thermo Fisher Scientific) for 15 min during gentle agitation at room temperature (RT), using a 2:1 v/v ratio of lysis buffer to PBS. The cell suspension was centrifuged (400 *g* for 5 min at 4°C) and cells were re-suspended in the L929-conditioned cell culture medium also used for mouse $M\Phi_{BM}$ colony stimulation.

A human atrial fibroblast (HAF) line that we characterised previously (Kunzel, Rausch et al., 2020), was cultured in DMEM supplemented with 2 mM L-alanyl-L-glutamine (GlutaMAX, Thermo Fisher Scientific, Darmstadt, Germany), 10% FBS and 1% penicillin/streptomycin, and used as a positive control for pharmacological interventions targeting MSC.

Patch-clamp recordings and mechanical stimulation

The patch-clamp technique was used to assess the activity of MSC in the plasma membrane. Cell-attached patch-clamp recordings were performed as previously described for characterising Piezo1 channels (Jakob, Klesen et al., 2021). The pipette solution contained (in mM): NaCl 150, KCl 5, $CaCl_2$ 2, and HEPES 10; pH 7.4 with NaOH, 310 mOsm/L, while the bath solution contained (in mM): KCl 155, EGTA 5, $MgCl_2$ 3, and HEPES 10; pH 7.2 with KOH, 310 mOsm/L (osmolality measured using a K-7400 osmometer; Knauer Wissenschaftliche Geräte, Berlin, Germany). Cells were washed twice with bath solution prior to recording, with at least 5 min between culture medium removal and the first recordings to avoid any potential blocking effects of antibiotics on MSC (Gannier, White et al., 1994). Membrane patches were stimulated with brief (500 ms) negative pressure pulses, applied via the patch pipette (average pipette resistance 1.2 MΩ) with 10 mmHg increments from 0 to −80 mmHg, using a pressure-clamp device (ALA High Speed Pressure Clamp-1 system; ALA Scientific, Farmingdale, NY, USA). Experiments were performed at RT (20°C), using a patch-clamp amplifier (200B, Molecular Devices, San Jose, CA, USA) and a Digidata 1440A interface (Molecular Devices). Currents were digitised at 3 kHz, low-pass filtered at 1 kHz, and analysed with pCLAMP10.3 (Molecular Devices) and OriginPro 2019 software (OriginLab Corp., Northampton, MA, USA).

Ca^{2+} imaging and signal analysis

Prior to imaging, cells were washed in Ca^{2+}-free PBS and incubated for 20 min at RT with 3 μM Fluo-4-AM (F14201, Thermo Fisher Scientific) in PBS while being protected from ambient light. From this step onwards, cells were no longer exposed to antibiotics. After 20 min, the loading solution was removed, cells were washed with

PBS and used for Ca^{2+} imaging within 5–10 min after exposure to a HEPES-buffered solution (in mM): NaCl 140, KCl 5.4, HEPES 10, glucose 10, $CaCl_2$ 1.8, $MgCl_2$ 1.0; pH 7.4 with NaOH, 300 mOsm/L.

Ca^{2+} dynamics in MΦ were imaged on an inverted confocal microscope (TCS SP8 X, Leica Microsystems, Wetzlar, Germany) using a ×40 water immersion objective (HC PL APO CS2 ×40/1.10) with a frame rate ranging from 40 to 46 images per minute. Fluo-4-AM was excited using a 488 nm laser line and the fluorescence signal was recorded with a hybrid detector operated in photon counting mode. The detection window was set from 497 to 568 nm. In order to maximise signal intensity, the pinhole was opened (7.33 Airy units). The Piezo1 channel activator Yoda1 (5, 10, 20 or 30 μM, diluted from a 10 mM stock solution in dimethyl sulfoxide (DMSO); Tocris Bioscience, Bristol, UK) and the TRPV4 agonist GSK1016790A (300 nM (Sigma-Aldrich) dissolved in HEPES-buffered solution) were applied using a local perfusion system. A vacuum-based suction system maintained a constant fluid volume in the dish (∼1.5 mL). Flow rate was set to 1 mL/min by adjusting the height of reservoirs for gravity-driven flow. The control solution for Yoda1 experiments contained DMSO equivalent to the largest Yoda1 concentration tested (0.3% v/v, both for patch-clamp and Ca^{2+} experiments).

Ca^{2+} signals were analysed with ImageJ. The StarDist plugin (Schmidt, Weigert et al., 2018) was used for cell area detection in images. Thereafter, mean pixel intensities were obtained for each time point to quantify temporal responses to Yoda1 and GSK1016790A. Data were exported to MATLAB (The MathWorks, Natick, MA, USA) for further processing. Following background subtraction and signal normalisation, baseline fluorescence was measured as the average of the last 10 frames before application of Yoda1 and GSK1016790A. To determine the maximal amplitude of responses to different treatments, the peak fluorescence signal reached during treatment exposure was selected for each cell.

RNA sequencing: expression of genes coding for mechanosensitive channels

The mRNA expression of MSC was assessed using published RNA sequencing data of murine $M\Phi_{BM}$ and $M\Phi_{TR}$ (Simon-Chica, Fernández et al., 2022; Xu, Gao et al., 2023). In brief, RNA-seq libraries from FACS-purified $M\Phi_{TR}$ were generated using 5 ng RNA per sample using the NuGEN Ovation SoLo RNA-seq System (Tecan, Chapell Hill, NC, USA). cDNA fragments of ∼350 bp were sonicated using a Bioruptor (Diagenode, Liege, Belgium), amplified by fluorescence-controlled PCR, and cDNA size was selected using AMPure XP Beads (Beckmann Coulter, Brea, CA, USA). Quality and mean fragment size of library samples were assessed using a bioanalyser (2100 Bioanalyzer, Agilent Technologies, Santa Clara, CA, USA). Finally, libraries were sequenced on Illumina sequencers in paired-end mode. Raw data sets on $M\Phi_{BM}$ were obtained from the National Centre for Biotechnology Information's sequence read archive (Gene Expression Omnibus accession numbers: GSM6506821, GSM6506822 and GSM6506823). Raw data on $M\Phi_{TR}$ were obtained from our previously published work (Simon-Chica, Fernández et al., 2022). All data were analysed using the Galaxy platform (Afgan, Baker et al., 2018). This involved pre-processing and mapping onto the murine reference genome (NCBI37/mm9) as previously described (Simon-Chica, Fernández et al., 2022). Gene expression in both datasets was assessed using featureCounts (Liao, Smyth & Shi 2014). The results were transformed into transcripts per kilobase million (TPM) taking into account gene length and sequencing depth. TPM of selected MSC were used as a measure of their expression at the mRNA level.

scRNA-seq data were obtained from cardiac cells isolated from left ventricular tissue slices (Greiner, Schiatti et al., 2022). Briefly, following blood removal by Langendorff perfusion, hearts were placed in a Petri dish (TPP, Trasadingen, Switzerland) filled with cold cutting solution, containing (in mM): NaCl 138, NaH_2PO_4 0.33, KCl 5.4, $MgCl_2$ 2, HEPES 10, glucose 10, $CaCl_2$ 0.5, 2,3-butanedione 2-monoxime (BDM) 30, pH adjusted to 7.3 with 1 M NaOH at 37°C, osmolarity 330 ± 10 mOsm/L. Tissue blocks of ventricular free wall containing the post-cryoablation lesion centre (identified as a region appearing mostly white), border zone and adjacent myocardium (or corresponding tissue areas from sham animals) were excised and embedded in low-melting-point agarose (4% (m/v)) at 37°C, and then put on ice. Agarose blocks were sliced with a precision vibratome (model 7000smz-2; Campden Instruments, Loughborough, UK). Slices, cut at a thickness of 300 μm, were stored at 4°C in cutting solution and warmed to RT before initiating cell isolation. The enzymatic solution contained (in mM): KCl 20, KH_2PO_4 10, $MgCl_2$ 2, Taurin 20, glucose 10, L-glutamic acid potassium salt monohydrate 100, BDM 30, pH adjusted to 7.3 with KOH at 37°C. Tissue was digested for 12 min with proteinase XXIV (concentration: 0.5 mg/mL in 2 mL; Sigma-Aldrich, St. Louis, MO, USA) and further digested with Liberase TL Research Grade (concentration: 0.23 mg/mL with 5 μM $CaCl_2$; Hoffmann-La Roche, Basel, Switzerland) for up to 45 min. Cells were stained with the Zombie-NIR viability dye (BioLegend, San Diego, CA, USA) and sorted in FACSAria™ III Cell Sorter (BD BioSciences) to enrich for living cells (Zombie-NIR negative gate). Sorted cells were encapsulated into emulsion droplets using the Chromium Controller (10× Genomics, Pleasanton, CA, USA) according to the manufacturer's instruction, and then sequenced on the Nextseq2000 platform (Illumina, San Diego, CA, USA).

The CellRanger v6.1.1. pipeline was used to generate a digital gene expression matrix starting from raw data. For alignment and quantification of gene expression the reference transcriptome has been built using the mouse mm10-2020-A as reference genome. Single cell clustering of macrophages and data analysis were performed using VarID2 (Rosales-Alvarez, Rettkowski et al., 2023). Only cells with more than 1000 unique molecular identifier counts were considered for clustering and analysis. For clustering, gene expression values were normalised by correcting variability associated with total transcript count per cell by a negative binomial regression (Rosales-Alvarez, Rettkowski et al., 2023). For data representation, count data were normalised by dividing transcript counts in each cell by the total transcript count per cell and multiplying by the minimum total transcript count across all cells.

Western blot analysis

Three days after transfecting HEK cells with plasmids encoding either enhanced green fluorescent protein (EGFP; negative control) or Piezo1 (vector backbone: pIRES2_EGFP, 6029-1, Addgene, Watertown, MA, USA), cells were lysed in radio immunoprecipitation buffer (containing (in mM): Tris–HCl 50 and NaCl 150; and (in % m/v) NP-40 1, sodium deoxycholate 1, and SDS 0.1) supplemented with protease inhibitors (1:200, 539134, Merck, Darmstadt, Germany) for 15 min on ice. Subsequently, lysates were subjected to SDS-PAGE using 7% polyacrylamide gels, and transferred to nitrocellulose membranes. These were saturated by incubation in 5% BSA in PBS for 1 h at RT. Primary antibodies against Piezo1 (generated in mouse, NBP2-75 617, isotype IgG2a, Novus Biologicals, Brussels, Belgium) or glyceraldehyde-3-phosphate dehydrogenase (generated in mouse, G8795, Sigma-Aldrich, Hamburg, Germany) were applied at a dilution of 1:1000 in 5% BSA overnight at 4°C with gentle agitation. Horseradish peroxidase-coupled secondary antibody (anti-mouse, HAF007, R&D Systems, Minneapolis, MN, USA) was applied at a dilution of 1:5,000. The signals were visualised using SuperSignal West Femto Maximum Sensitivity Substrate (34096, Thermo Fisher Scientific), and recorded using a Fusion-Fx gel documentation system (Vilber, Eberhardzell, Germany).

Immunocytochemistry

HAF were seeded at 50,000 cells/mL on uncoated glass coverslips. They were fixed (10 min) with paraformaldehyde (4%), treated with blocking buffer (PBS, 10% goat serum) and then incubated overnight at 4°C with the anti-Piezo1 primary antibody (NBP2-75617, isotype IgG2a, Novus Biologicals) at a dilution of 1:500 (antibody dilution in PBS, 1% BSA, 2.5% FBS). The secondary antibody, goat anti-mouse IgG2a tagged with Alexa Fluor 555 (Thermo Fisher Scientific, product reference A-21137) was diluted at 1:500 in PBS, and samples were incubated for 1 h at RT with continuous agitation (orbital shaker, homemade). Nuclei counterstaining was performed with Hoechst 33342, dilution 1:1000 in PBS. Imaging was performed on a TCS SP8 X microscope (Leica Microsystems). To test the specificity of the primary antibody, Piezo1 was knocked down using a set of siRNA (SMARTpool, Dharmacon, Lafayette, CO, USA) as previously reported (Jakob, Klesen et al., 2021). Seventy-two hours after siRNA treatment cells were used for qPCR or fixed in 4% paraformaldehyde in PBS for immunocytochemistry. Fluorescently labelled cells were segmented using cellpose (Pachitariu & Stringer 2022; Stringer, Wang et al., 2021). The model was trained using the mean intensity of all fluorescence signals as cytoplasmic channel and the Hoechst staining as nuclear channel. We iteratively retrained with manual annotations in a human-in-the-loop approach, starting from the 'cyto2' model and using the graphical user interface supplied with the cellpose package. An interactive website developed with Bokeh (bokeh.org) provided both stack-level and cell-level visualisations, and was used for inspecting segmentations, and selecting stacks for manual annotations. Cells truncated at image boundaries were excluded from the analysis.

Statistical analysis

Data distribution was assessed with the Shapiro–Wilk normality test. Normally distributed data were compared using Student's *t* test, and non-normally distributed data were compared using the Mann–Whitney test or the Kruskal–Wallis test. Data are expressed as means ± SEM, individual data points are shown to illustrate the variability, and P-values <0.05 are considered as indicative of statistically significant differences between means. Throughout the study, '*N*' refers to the number of animals and '*n*' to the number of cells.

Results

Stretch-induced inward currents are observed in $M\Phi_{BM}$ and $M\Phi_{TR}$

We compared the mechanical responses of murine isolated ventricular cardiac $M\Phi_{TR}$ to cultured $M\Phi_{BM}$. To assess the presence of stretch-induced currents, we performed cell-attached patch-clamp recordings, while steps of negative pressure were applied via the recording pipette to locally stretch the cell membrane (Fig. 1*A*). We

found stretch-induced inward currents in 67% of murine $M\Phi_{BM}$ ($N = 4$, $n = 40$ out of 60) and 56% of $M\Phi_{TR}$ ($N = 6$, $n = 30$ out of 54; Fig. 1*B*). Pressure steps swiftly activated currents with no pronounced inactivation and slow deactivation. Quantification of the mean currents (calculated over the duration of the pulse of pressure) across the patched membrane as a function of applied pressure is shown in Fig. 1*C*. Mean currents measured during maximum pressure pulses (−80 mmHg) were 17.7 ± 4.9 pA and 10.3 ± 2.2 pA for mouse $M\Phi_{BM}$ and $M\Phi_{TR}$, respectively. When comparing stretch-activated current amplitudes across all tested pressure values, we found significantly higher current amplitudes in $M\Phi_{BM}$ compared to $M\Phi_{TR}$ at −30 mmHg ($P = 0.036$) and −80 mmHg ($P < 0.0001$), but not at other pressures. Comparable stretch-induced current profiles were also detected in $M\Phi_{BM}$ from pigs (Fig. 1*D* and *E*). Taken together, the inward currents elicited by negative pressure application indicate the presence of functional MSC in plasma membranes of $M\Phi_{BM}$ and $M\Phi_{TR}$.

Stretch-induced currents show characteristics of cation non-selective MSC

In a subset of recorded MΦ membrane patches, we were able to discern individual channel opening events. Representative current traces at −20 mmHg and −120 mV are shown in Fig. 2*A*. For further characterisation, we assessed single-channel current amplitudes at holding potentials from −120 mV to −40 mV. Current−voltage curves were fitted by linear regression, with the slopes corresponding to single channel conductances of 38.3 ± 0.2 pS and 44.3 ± 0.1 pS for $M\Phi_{BM}$ and $M\Phi_{TR}$, respectively ($P = 0.73$, Mann–Whitney test). The reversal potentials, obtained by linear extrapolation, were 0.5 mV (−14.3 to 22.5 mV, 95% confidence interval) and −10.7 mV (−22.0 to 4.8 mV) for $M\Phi_{BM}$ and $M\Phi_{TR}$, respectively. We also assessed current responses to repeat application of −80 mmHg pressure pulses and found a decline in current amplitudes during repetitive stimulation (Fig. 2*B*). Normalised current amplitudes decay mono-exponentially with a half-maximal reduction after six to eight iterations of negative pressure application (Fig. 2*C*; $M\Phi_{BM}$ $N = 2$, $n = 6$, $M\Phi_{TR}$ $N = 2$, $n = 5$). These data support the hypothesis that cation non-selective MSC are present and active in both types of MΦ.

MΦ express RNA coding for multiple MSC, including Piezo1

In order to identify molecular candidates that may underlie the observed stretch-induced currents, we analysed RNA expression levels in freshly isolated $M\Phi_{TR}$ and

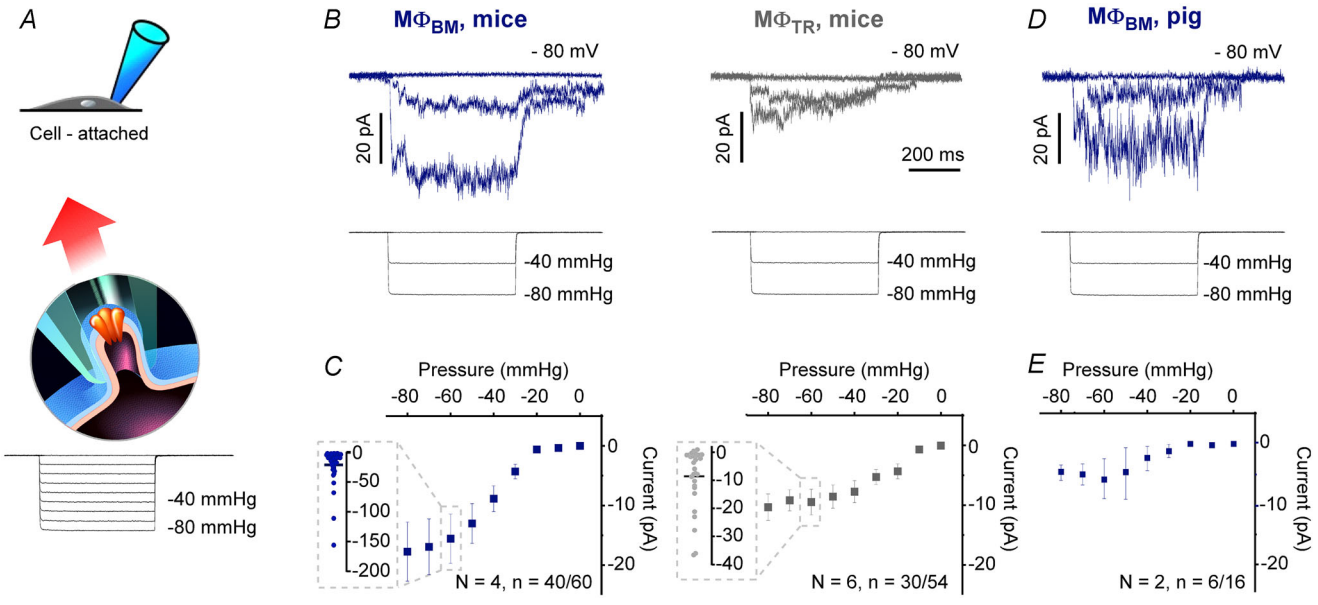

Figure 1. MSC in murine $M\Phi_{BM}$ and cardiac $M\Phi_{TR}$
A, schematic representation of the cell-attached patch-clamp method used to investigate the presence of MSC (adapted from F. Aguila (CNRS), with permission). Bottom trace illustrates the pressure pulse protocol applied from 0 to −80 mmHg in 10 mmHg steps. *B*, representative traces of currents at 0, −40 and −80 mmHg (pressure protocol illustrated by the bottom traces) in $M\Phi_{BM}$ (blue, N = 4 independent experiments/animals, n = 40/60 responsive cells/total number of recorded cells) and $M\Phi_{TR}$ (grey, N = 6, n = 30/54). Holding potential −80 mV. *C*, current−pressure relationships at a holding potential of −80 mV in $M\Phi_{BM}$ isolated from mice (n = 40 cells) and in $M\Phi_{TR}$ (n = 30 cells). *D* and *E*, same as in *B* and *C* but using pig $M\Phi_{BM}$. Results are shown as means ± SEM.

compared them to RNA expression data for $M\Phi_{BM}$. We focused on the expression of genes coding for MSC in the broadest sense, including 'mechanically modulated' (responding indirectly to mechanical stimulation or requiring co-activation) and 'mechanically gated' ion channels (changing their open probability in direct response to mechanical stimulation; see (Peyronnet, Nerbonne & Kohl 2016) for detail on nomenclature). We also included MSC candidates, i.e. ion-conducting pathways that have not yet been functionally confirmed to be mechanosensitive, but which are predicted to be mechanosensitive – based on phylogenetic analyses and sequence similarity, e.g. number of transmembrane domains of the corresponding proteins and/or links with mechanotransduction pathways. The 20 most highly expressed genes coding for the thus-demarcated MSC in $M\Phi_{BM}$ and $M\Phi_{TR}$ are presented in Fig. 2*D* and *E*, respectively. Out of these, 14 genes were highly expressed in both $M\Phi_{BM}$ and $M\Phi_{TR}$ (Fig. 2*F*).

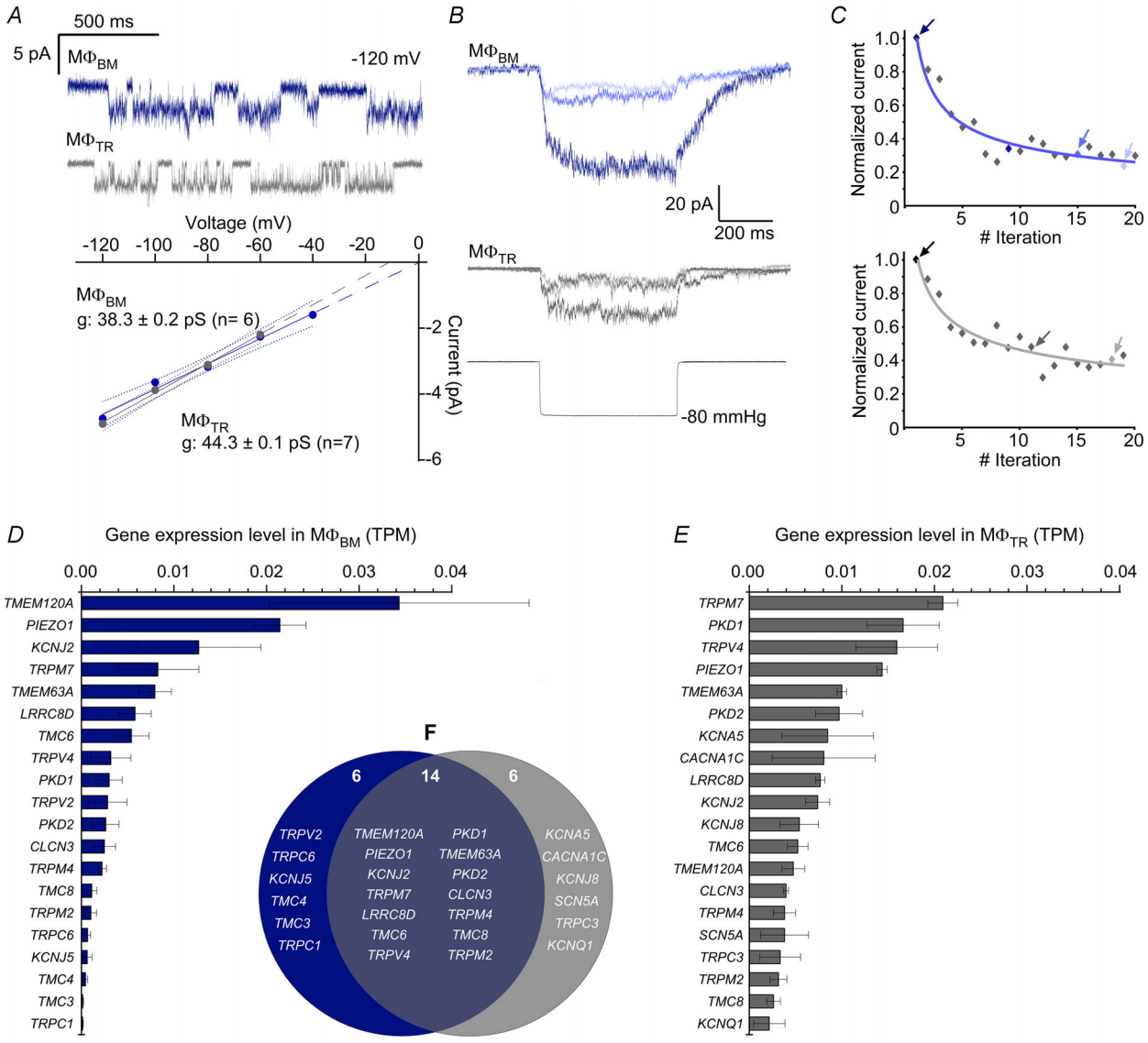

Figure 2. Biophysical characterisation of MSC in murine $M\Phi_{BM}$ and cardiac $M\Phi_{TR}$
A, example traces of single channel activities from $M\Phi_{BM}$ in blue and $M\Phi_{TR}$ in grey, recorded at −20 mmHg and at a holding potential of −120 mV (top). Current–voltage relationships for single channel currents. The slope of the linear regression identifies channel conductance (confidence intervals are shown). *B*, repetitive pressure stimulations (−80 mmHg) induced current run-down at −80 mV in $M\Phi_{BM}$ (blue) and $M\Phi_{TR}$ (grey); the lighter the colour, the higher the iteration number. *C*, normalised decrease in mean current *vs*. number of pressure pulse iteration in $M\Phi_{BM}$ and $M\Phi_{TR}$. Data points corresponding to the traces shown in *B* are marked with an arrow. *D* and *E*, RNA-seq data from $M\Phi_{BM}$ and $M\Phi_{TR}$ showing levels of mRNA coding for mechanosensitive channels. *F*, MSC expressed in $M\Phi_{BM}$ or in $M\Phi_{TR}$ or in both. TPM: transcripts per kilobase million.

Based on the biophysical characterisation in the section 'Stretch-induced currents show characteristics of cation non-selective MSC', the most plausible candidates underlying stretch-induced currents seen in MΦ are genes coding for cation non-selective MSC. Among the most highly expressed genes in $M\Phi_{BM}$ and $M\Phi_{TR}$, those would include *PIEZO1* (Fig. 2*D*, *E* and Supporting information Fig. S1), several TRP channels from the melastatin (*TPRM7*), the polycystin (*TRPP1* and *2*), and the vanilloid (*TRPV4*) families, as well as the recently identified MSC TACAN (*TMEM120A*; Fig. 2*D* and *E*) (Beaulieu-Laroche, Christin et al., 2020).

Yoda1 increases stretch-induced currents in $M\Phi_{BM}$, but not in $M\Phi_{TR}$

As Piezo1 has been shown before to play a role in mechanosensation in murine monocytes and $M\Phi_{BM}$ (Atcha, Jairaman et al., 2021), we tested effects of the Piezo1 agonist Yoda1 on MSC activity in murine $M\Phi_{BM}$ and cardiac $M\Phi_{TR}$. In $M\Phi_{BM}$, addition of 30 μM Yoda1 (the maximum concentration that could reliably be dissolved) to the pipette solution resulted in a higher average amplitude of stretch-induced currents (42.8 ± 6.3 pA, $N = 3$, $n = 19$; at −60 mmHg) compared to control conditions without Yoda1 (13.9 ± 2.2 pA, $N = 4$, $n = 40$; $P < 0.0001$, Mann–Whitney test, Fig. 3*A*). In contrast, stretch-induced currents recorded from $M\Phi_{TR}$ were not significantly affected by addition of 30 μM Yoda1 (9.9 ± 1.9 pA, $N = 4$, $n = 24$) compared to control recordings without the agonist (9.5 ± 1.8 pA, $N = 6$, $n = 30$; $P = 0.564$, Mann–Whitney test, Fig. 3*B*).

Yoda1 increases cytosolic Ca^{2+} levels in $M\Phi_{BM}$ only, while GSK1016790A increases Ca^{2+} levels in both $M\Phi_{BM}$ and $M\Phi_{TR}$

We monitored cytosolic Ca^{2+} concentration using the high-affinity fluorescent dye Fluo-4-AM as a complementary and more integrated readout to visualise

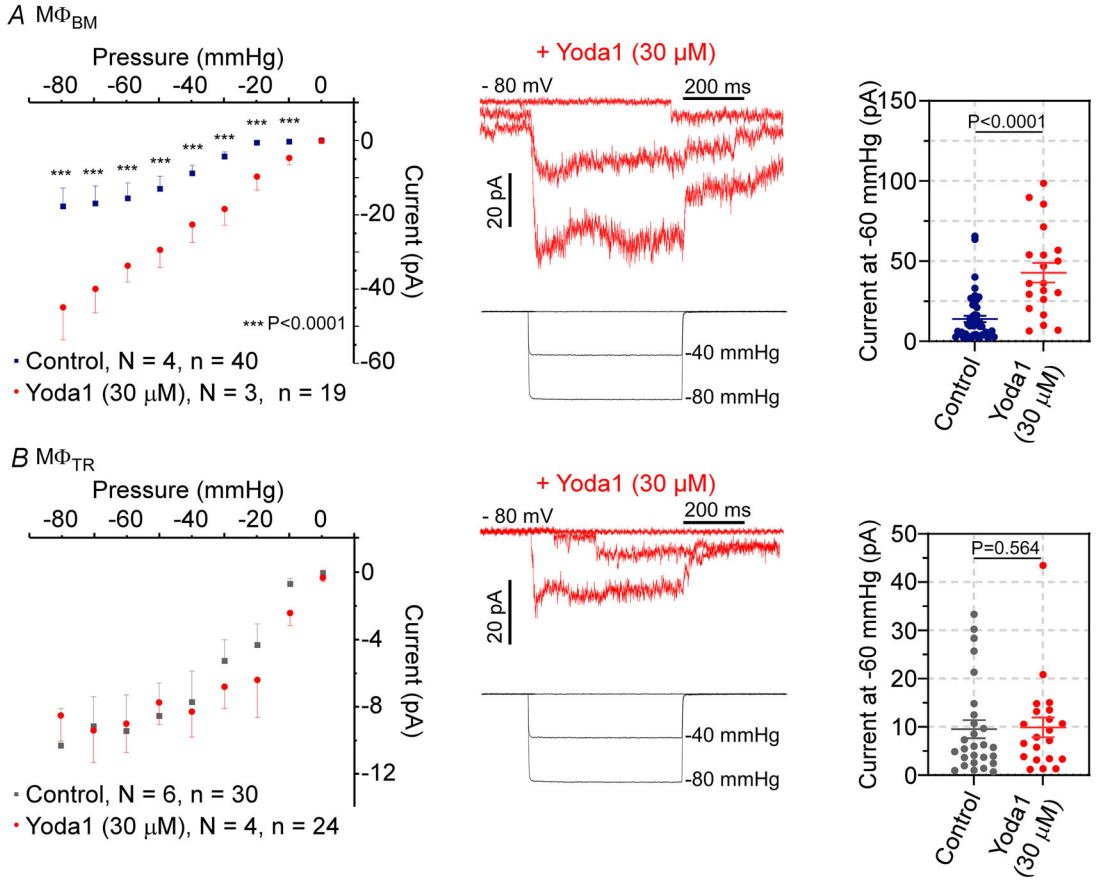

Figure 3. Effect of Piezo1 agonist Yoda1 on MSC activity in $M\Phi_{BM}$ and $M\Phi_{TR}$
A, mean current amplitudes elicited by negative pressure pulses in cell-attached patch-clamp mode in $M\Phi_{BM}$ in the absence (blue, $N = 4$, $n = 40$ cells) and presence (red, $N = 3$, $n = 19$ cells) of 30 μM Yoda1. *B*, mean current amplitudes elicited by negative pressure pulses in $M\Phi_{TR}$ in the absence (grey, $N = 6$, $n = 30$ cells) and presence (red, $N = 4$, $n = 24$ cells) of 30 μM Yoda1. All measurements at −80 mV. Error bars indicate SEM. Mann–Whitney test was used for statistical assessment of differences.

potential Yoda1 effects on Piezo1 activity at the whole-cell level and in a larger number of cells (Fig. 4*A*). Extracellular application of 10 and 30 μM Yoda1 via the local perfusion stream induced a significant increase in fluorescence of Fluo-4-loaded $M\Phi_{BM}$, indicating a rise in cytosolic Ca^{2+} concentration compared to control conditions ($N = 2$, $n = 222$, 190 or 632 cells for 5, 10 and 30 μM Yoda1, respectively, and $n = 173$ for DMSO-containing control; Fig. 4*B*). The Yoda1-induced increase in fluorescence was transient (Fig. 4*C*).

In $M\Phi_{TR}$, we did not observe a significant increase in Fluo-4 fluorescence upon exposure to 20 μM Yoda1 ($N = 2$, $n = 50$; Fig. 5*A*–*C*). As the application of the Piezo1 agonist Yoda1 did not significantly affect stretch-induced currents or cytosolic Ca^{2+} concentration in $M\Phi_{TR}$, we tested an agonist targeting TRPV4, which, like Piezo1, is cation non-selective and strongly expressed in $M\Phi_{TR}$ (Fig. 2*E*). Application of the selective agonist GSK1016790A (300 nM) gave rise to a large and reversible increase in Fluo-4 fluorescence in $M\Phi_{TR}$ ($N = 2$, $n = 110$; Fig. 5*A*–*C*), indicating that TRPV4 is active in $M\Phi_{TR}$. For comparison, we also tested the effect of GSK1016790A on $M\Phi_{BM}$. We observed a significant increase in cytosolic Ca^{2+} levels in $M\Phi_{BM}$, which, however, was significantly smaller ($P < 0.0001$) than the increase in Ca^{2+} levels observed upon application of 20 μM Yoda1 (Fig. 5*D*–*F*).

To assess Piezo1 protein expression in $M\Phi_{BM}$ and $M\Phi_{TR}$, we performed Piezo1 immunolabelling for Western blot analysis, fluorescence imaging and flow cytometry (Supporting information, Fig. S2). However, given the unspecific binding of the commercially available Piezo1 antibody, observed in Western blot data and in confocal imaging experiments, data interpretation was inconclusive.

Ventricular cryoablation does not significantly change stretch-induced current amplitudes of $M\Phi_{TR}$ nor the relative number of cells responsive to Yoda1

We assessed Piezo1 activity in cardiac MΦ, isolated from murine hearts 21–28 days after ventricular cryoablation, assuming that these contain a mix of tissue-resident and recruited cells. We assessed stretch-induced currents in response to Yoda1 in left ventricular MΦ from tissue that was remote to the scar (Fig. 6*A*) and in the scar (Fig. 6*B*), and compared this to left ventricular $M\Phi_{TR}$ isolated from sham-operated littermates (Fig. 6*C*). In all tested conditions, Yoda1 did not induce a significant difference in whole-cell stretch-induced current amplitudes compared to control solution (Fig. 6*D*), nor in the relative number of cells showing stretch-induced currents upon Yoda1 application (Fig. 6*A*–*C*). In addition,

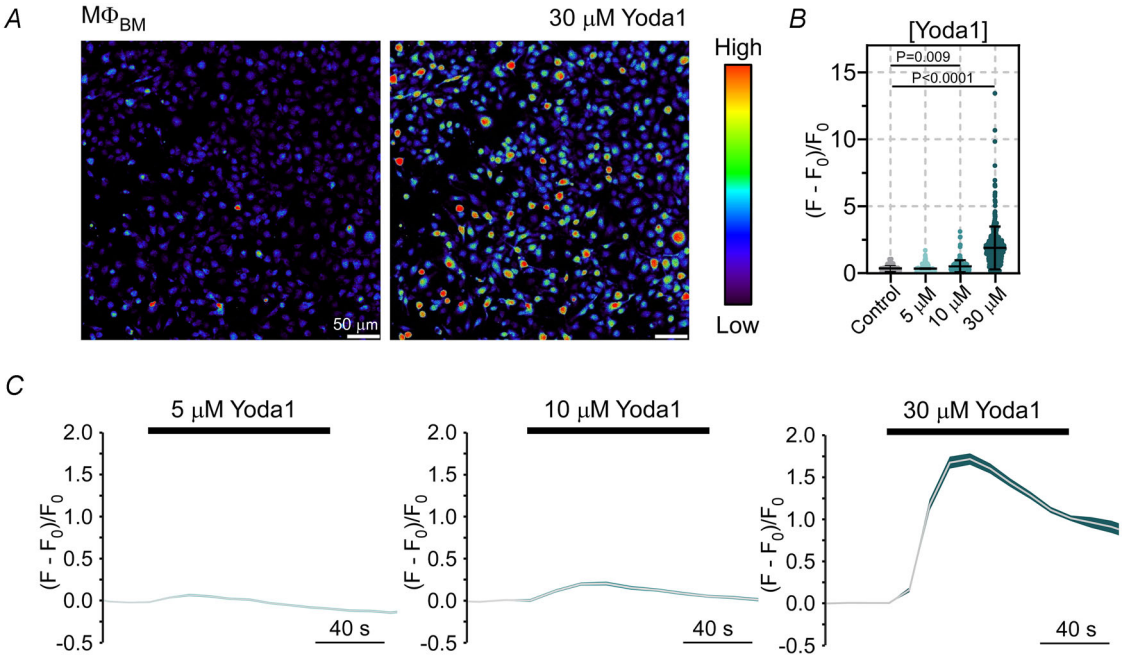

Figure 4. Cytosolic Ca^{2+} levels in murine $M\Phi_{BM}$ in response to Yoda1
A, representative images showing Fluo-4 fluorescence intensity before and after exposure to 30 μM Yoda1 (peak intensity). *B*, quantification of peak intensities per cell when exposed to DMSO (control; $N = 2$, $n = 173$ cells) or various concentrations of Yoda1 (5, 10 and 30 μM; $N = 2$, $n = 222$, 190 and 632 cells, respectively). *C*, time courses of normalised fluorescence signals averaged across all cells comparing exposure to 5, 10 and 30 μM Yoda1. Grey lines represent mean values and shaded regions SEM. Kruskal–Wallis test was used for assessment of statistically significant differences.

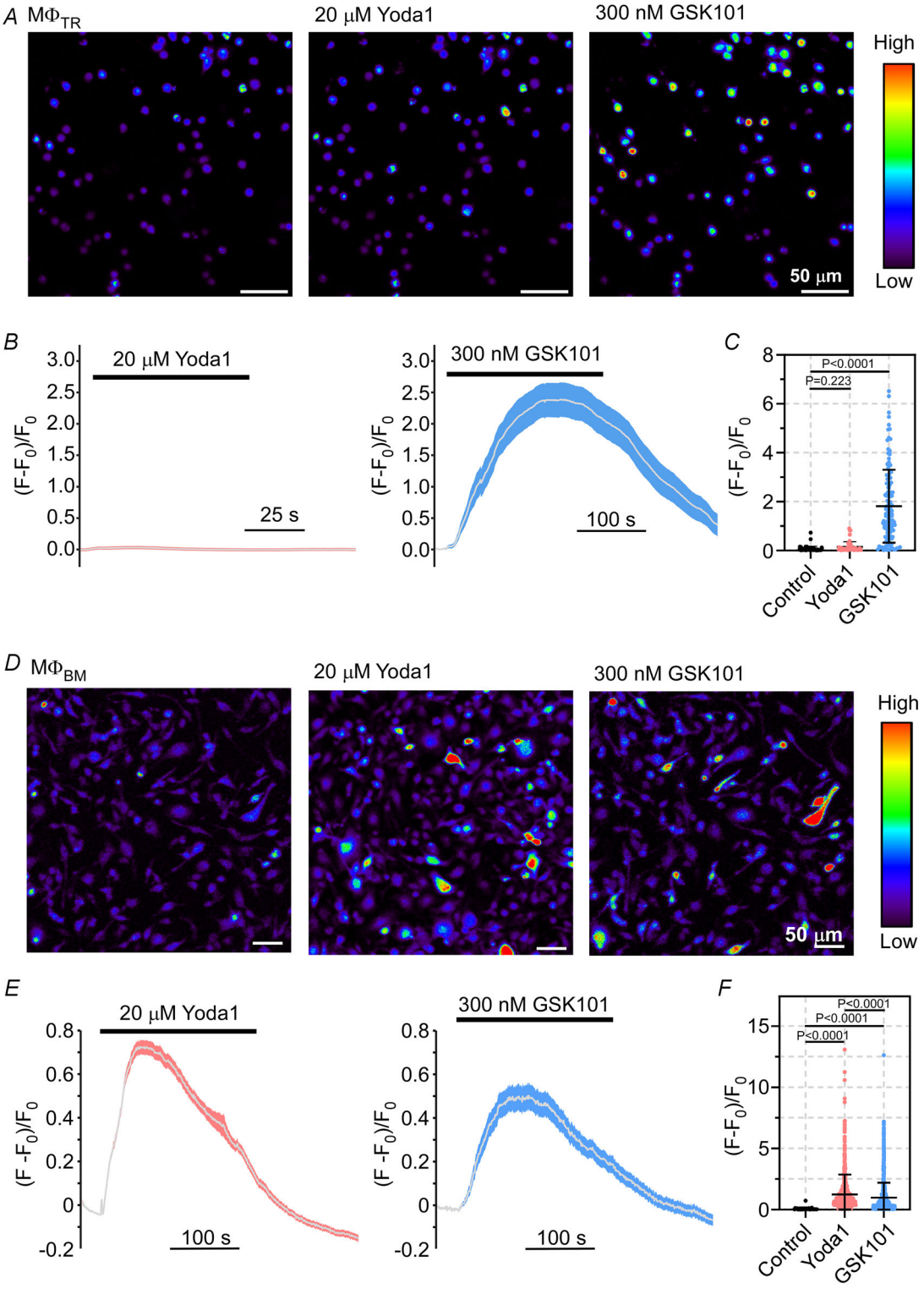

Figure 5. Ca^{2+} influx in murine $M\Phi_{TR}$ and $M\Phi_{BM}$ upon application of Piezo1 and TRPV4 activators
A, representative images showing Fluo-4 fluorescence intensity before and during exposure of $M\Phi_{TR}$ to 20 μM Yoda1 or 300 nM GSK101 (peak intensity). *B*, time courses of normalised fluorescence signals averaged across all cells comparing application of 20 μM Yoda1 to application of 300 nM GSK101. Grey lines represent mean values and shaded regions SEM. *C*, quantification of peak intensities per cell (N = 2 for each condition; n = 57, 50 and 110 cells in control conditions and in response to 20 μM Yoda1 and 300 nM GSK101, respectively). *D*, Representative images showing Fluo-4 fluorescence intensity before and after exposure of $M\Phi_{BM}$ to 20 μM Yoda1

or to 300 nM GSK101 (peak intensity). *E*, time courses of normalised fluorescence signals averaged across all cells comparing application of 20 μM Yoda1 to application of 300 nM GSK101. Grey lines represent mean values and shaded regions SEM. *F*, quantification of peak intensities per cell (N = 2; n = 25, 1215 and 1435 cells in control conditions and in response to 20 μM Yoda1 and 300 nM GSK101, respectively). GSK101 stands for GSK1016790A. Kruskal–Wallis test was used for assessment of differences between experimental groups.

scRNA-seq analyses showed that *Piezo1* expression was not significantly different when comparing MΦ isolated from hearts harvested at days 1 and 28 after cryoinjury to $MΦ_{TR}$ isolated from hearts of sham-operated mice, when all MΦ harvested are included (Fig. 6*E* and *F*). Interestingly, *Trpv4* was expressed at a lower level on day 1 in MΦ from cryoinjured ventricles, compared to sham-operated animals, a difference that is not detected after 28 days (Fig. 6*G* and *H*).

scRNA-seq data from left ventricular tissue slices comprising scar centre, border zone and adjacent myocardium show that on day 28 after sham surgery, 58% of isolated MΦ were *Timd4*$^+$, i.e. representing locally self-renewing MΦ; compared to 42% *Ccr2*$^+$ MΦ, derived from circulating monocytes (N = 2). On day 28 after cryoinjury we found 51% of isolated MΦ to be *Timd4*$^+$ compared to 49% *Ccr2*$^+$ MΦ (N = 5). When exploring *Piezo1* and *Trpv4* expression in these subpopulations, we found lower *Piezo1* (P = 0.044) and *Trpv4* (P < 0.0001) expression levels in *Ccr2*$^+$ MΦ on day 28 after surgery compared to *Timd4*$^+$ cells (Fig. 7). However, probably due to the only modest change in left ventricular tissue composition in respect to MΦ sub-populations, no significant differences in MSC activity were observed between MΦ isolated from hearts 21–28 days after either sham operation or cryoinjury (Fig. 6).

Discussion

MΦ contribute not only to maintenance of cardiac homeostasis, but also to tissue repair, such as during scar formation following myocardial injury. In the heart, $MΦ_{TR}$ are exposed to rhythmically changing mechanical forces during the cardiac contraction–relaxation cycle.

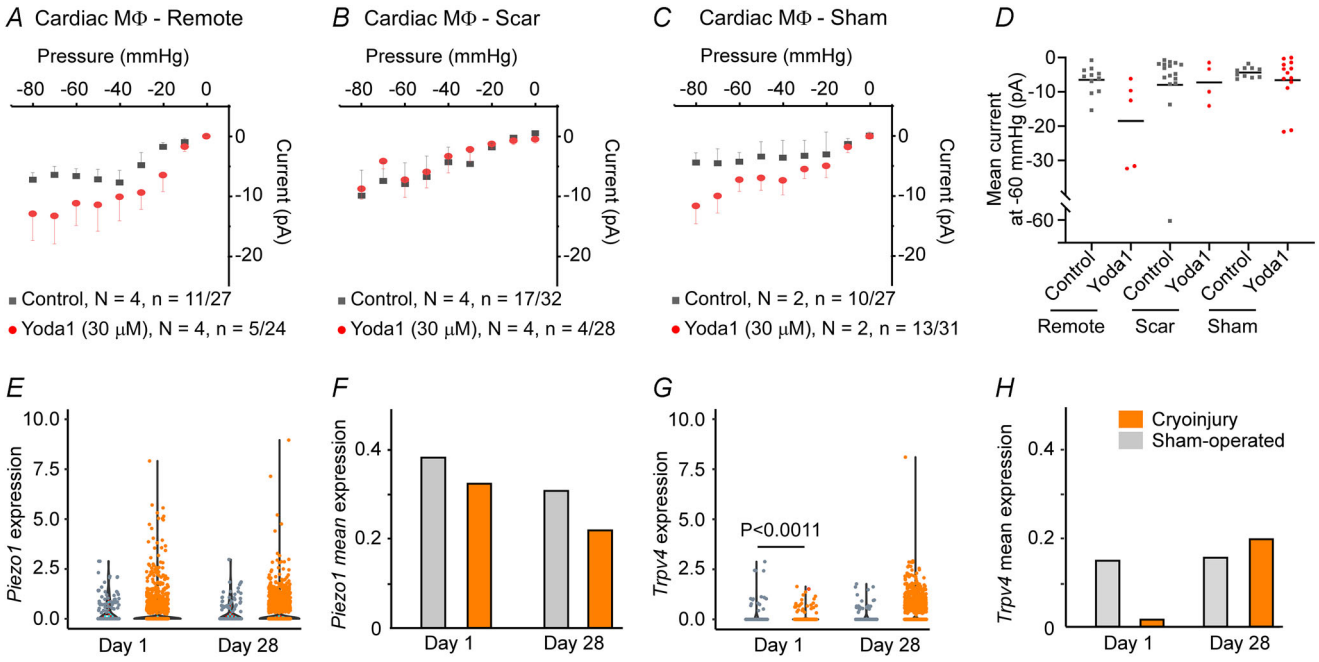

Figure 6. Effects of ventricular cryoinjury on MSC activity and expression levels in cardiac MΦ
A–C, Yoda1 effects on stretch-induced whole-cell currents in MΦ after cardiac injury, comparing MΦ isolated on days 21–28 after ventricular cryoinjury to MΦ isolated from sham-operated mice. Current–pressure relationships at a holding potential of −80 mV in MΦ isolated from regions remote to the scar (*A*), from the scar area (*B*), and from the corresponding ventricular regions of sham-operated animals (*C*) in the absence (grey) or presence (red) of Yoda1 (30 μM) in the pipette solution. *D*, current amplitude of individual cells at −60 mV. *E–H*, quantification of *Piezo1* and *Trpv4* mRNA expression levels in single cells on day 1 and day 28 after intervention, comparing MΦ from mice that had undergone ventricular cryoablation and sham surgery. Log-transformed normalised counts (*E*, *G*) and mean expression levels (*F*, *H*), N = 2 hearts for sham surgery for each time point; n = 145 cells for day 1; 127 cells day 28) and N = 5 hearts for cryoinjury for each time point (n = 1368 cells for day 1; 2844 cells for day 28). Kruskal–Wallis test was used for assessment of differences between experimental groups.

Additionally, the mechanical environment of $M\Phi_{TR}$ is altered during cardiac scar formation, associated with inhomogeneous tissue stiffening, which in turn changes regional tissue deformation, stretch and shear forces. In contrast to $M\Phi_{BM}$ and circulating monocytes, little is known about the ability of cardiac $M\Phi_{TR}$ to sense and respond to mechanical stimuli. This study compares the activity of MSC in mouse $M\Phi_{BM}$ to cardiac $M\Phi_{TR}$. Our main findings are: (1) $M\Phi_{BM}$ and $M\Phi_{TR}$ have stretch-induced currents, indicating functional expression of MSC in their plasma membrane; (2) current profiles are comparable between $M\Phi_{BM}$ and $M\Phi_{TR}$, showing characteristics of cation non-selective MSC; (3) unlike in $M\Phi_{BM}$, Piezo1 ion channel activity in the plasma membrane of $M\Phi_{TR}$ is not detectable; and (4) stretch-induced current profiles are not significantly different in MΦ isolated from post-ablation tissue compared to MΦ isolated from remote or healthy control myocardium.

$M\Phi_{BM}$ and $M\Phi_{TR}$ express functional MSC

We confirm the presence of stretch-induced currents in murine $M\Phi_{BM}$, and report similar current profiles in murine cardiac $M\Phi_{TR}$. Macroscopic current amplitudes (for the whole patch) do not differ significantly between the tested MΦ populations, except for pressure pulses at −30 mmHg and at −80 mmHg, and current kinetics share fast activation, no or weak inactivation, and slow deactivation. Observed currents are inwardly directed at negative membrane voltages, with extrapolated reversal potentials in the range between −10 mV and 0 mV for $M\Phi_{BM}$ and $M\Phi_{TR}$. Together, these data confirm functional expression of cation non-selective MSC in the plasma membrane of $M\Phi_{BM}$ and $M\Phi_{TR}$. Additionally, we were able to record single channel activity in some membrane patches, and estimated single channel conductances in the range of 38–44 pS for $M\Phi_{BM}$ and $M\Phi_{TR}$, respectively. The observed biophysical properties are shared by a number of mechanosensitive ion channels, including members of the TRP family and Piezo channels. This is in keeping with own and previously published RNA sequencing data, which shows that $M\Phi_{BM}$ and $M\Phi_{TR}$ express mRNA coding for TRPV, TRPM, TRPP and Piezo1 channels, albeit at different levels. The activity of MSC in pig $M\Phi_{BM}$ and the previously reported presence of Piezo1 in human non-cardiac MΦ (Tang, Zhao et al., 2023) support the translational relevance of MSC for mechanosensation of MΦ across species, and further studies are required to assess their activity in cardiac MΦ of large animal models and ultimately in human.

Direct comparison of RNA expression data from $M\Phi_{BM}$ and $M\Phi_{TR}$ should be considered with caution, due to differences between protocols used to obtain the cells. We tried to control these differences in functional studies, and recorded all MΦ within the same time window after plating them (5–30 h). That said, $M\Phi_{BM}$ were cultured and differentiated for 7 days before plating, while $M\Phi_{TR}$ were obtained acutely by enzymatic digestion, and then sorted (FACS) and plated.

Despite presence of mRNA transcripts, Piezo1 channel activity was not detected in $M\Phi_{TR}$

RNA sequencing data reveal that Piezo1 mRNA is expressed in $M\Phi_{BM}$ and $M\Phi_{TR}$, in keeping with another recent study (Lother, Bondareva et al., 2021). However, while the application of the Piezo1-specific agonist Yoda1 increased stretch-induced currents, leading to a transient rise in the intracellular Ca^{2+} levels in $M\Phi_{BM}$, Yoda1 application did not affect significantly either current amplitudes or Ca^{2+} concentrations in isolated cardiac $M\Phi_{TR}$. The apparent discrepancy between mRNA levels

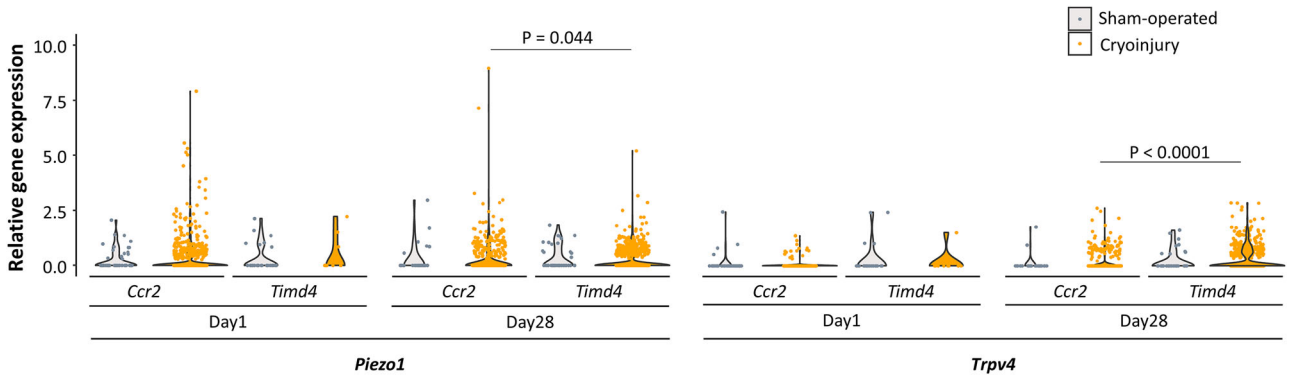

Figure 7. *Piezo1* and *Trpv4* expression, represented by log-transformed normalised counts across resident (*Timd4*$^+$) and recruited (*Ccr2*$^+$) macrophages, 1 and 28 days after cryoinjury
N = 2 hearts for sham surgery per time point (*n* = 53 cells for *Ccr2*$^+$ MΦ and *n* = 74 cells for *Timd4*$^+$ MΦ) and *N* = 5 hearts for cryoinjury per time point (*n* = 1404 cells for *Ccr2*$^+$ MΦ and *n* = 1440 for *Timd4*$^+$ MΦ). Kruskal–Wallis test was used for assessment of differences in expression levels.

and functional experiments may be explained by Piezo1 localisation on intracellular membranes, rather than the plasma membrane. Such endomembrane localisation of Piezo1 has been described for the endoplasmic reticulum of epithelial cells (McHugh, Buttery et al., 2010) and for the endoplasmic/sarcoplasmic reticulum, mitochondria and nucleus of vascular smooth muscle cells (Liao, Lu et al., 2021). Furthermore, as $M\Phi_{TR}$ form a heterogeneous population, Piezo1 could be expressed in a sub-population of $M\Phi_{TR}$ only that may not be dominant in the cultures used for this study. This would be in line with the observation in monocytes that Piezo1 is present only in a unique $CD11b^+/CD115^+$ subpopulation, representing about 25–40% of the overall monocyte population under the conditions of the respective study (Forget, Gianni-Barrera et al., 2019). However, our previous study (Lother, Bondareva et al., 2021) showed that Piezo1 is expressed both in $CD45.2^+$ $CD11b^+$ cells with high F4/80 and low Ly6C expression (macrophages), and in cells with low F4/80 and high Ly6C expression (monocytes), making this hypothesis unlikely. An alternative explanation for the observed discrepancy is that plasma membrane-localised channel proteins may be affected by the cell isolation procedure, including treatment with collagenase I and XI, which is necessary to obtain $M\Phi_{TR}$ but not $M\Phi_{BM}$. That said, the same cell isolation protocol was used in a previous study where levels of K^+ channel-encoding mRNA matched structural observations and K^+ channel activity in $M\Phi_{TR}$ (Simon-Chica, Fernández et al., 2022). In addition, Piezo1-mediated Ca^{2+} signals were still visible in freshly isolated cells (cardiomyocytes) after an isolation protocol similar to the one used here to obtain $M\Phi_{TR}$ (also using collagenases) (Jiang, Yin et al., 2021). In the case of Piezo1, lack of a reliable antibody, as shown by Western blot analysis and confocal imaging of immunolabelled cells (Supporting information, Fig. S2), currently impedes validation of protein expression and assessment of the subcellular localisation of Piezo1. Additionally, the current study used cells plated on a stiff substrate (glass), and substrate mechanical properties may alter Piezo1 expression and/or activity as previously reported (Chen, Wanggou et al., 2018).

Yoda1 effects are different in patch-clamp recordings compared to Ca^{2+} imaging experiments

Currently, Yoda1 is the most commonly used agonist to pharmacologically activate both murine and human Piezo1 channels, affecting the sensitivity and inactivation kinetics of mechanically induced currents (Syeda, Xu et al., 2015). In the present study, we observed differential effects of Yoda1 in patch-clamp recordings compared to Ca^{2+} imaging experiments. In cell-attached patch-clamp recordings, addition of Yoda1 to the pipette solution does not induce large Piezo1 activity at baseline, but increases current amplitudes in the presence of additional mechanical stimulation (observations by us and others, and not limited to MΦ). Thus, in patch-clamp recordings, Yoda1 mainly sensitises Piezo1 to stretch, rather than activating channel gating in control conditions. In contrast, bath perfusion with Yoda1 is sufficient to induce an increase in cytosolic Ca^{2+} concentration, as observed by fluorescence imaging. These differential effects of Yoda1 application may be based on the different mechanical environments that the cell membrane exposed to Yoda1 faces in the different experiments. In the cell-attached mode (settings used to stretch and record the activity of Piezo1), recorded channels sit in a membrane patch surrounded by the small opening of the glass pipette, thereby creating a particular mechanical environment even before additional stretch application (inducing high membrane tension, changing membrane curvature, possibly shifting lipid and protein composition, and minimising flow-based shear) (Suchyna, Markin & Sachs 2009). This particular mechanical state may change the reference level of Piezo1 activity at rest or Yoda1 sensitivity compared to Ca^{2+} experiments in which Piezo1 mechanical environment is not disturbed by the pipette and where cells are exposed to fluid shear. Additionally, as highlighted above and elsewhere (Liu, Hu et al., 2022), Ca^{2+} imaging may also reveal Piezo1-mediated Ca^{2+} release from intracellular stores, which is not detectable with patch-clamp recordings of plasma membrane activity. Although the mechanisms underlying the apparently different effects of Yoda1 in patch-clamp *vs.* Ca^{2+} imaging are not currently known, Yoda1 consistently increased MSC activity in $M\Phi_{BM}$, but not in $M\Phi_{TR}$ in the current study.

Piezo1 may be functionally coupled to secondary ion channels

RNA sequencing data show expression of a wide array of mechanosensitive channels, including various TRP channels, in $M\Phi_{BM}$ and $M\Phi_{TR}$. This is in line with previous studies reporting the expression and activity of several members of the TRP family (including TRPM2/4/7/8, TRPC1/3/6 (canonical), TRPV1/2/4, TRPA1 (ankyrin), TRPM1/2/3 (mucolipins) and TRPP2) in myeloid cells. These channels have been implicated in the control of cell proliferation and survival, polarisation, mobility, phagocytosis, intercellular communication and inflammatory responses (as reviewed in: Santoni, Morelli et al., 2018; Selezneva, Gibb & Willis 2022).

We find that pharmacological activation of TRPV4 leads to a strong increase in cytosolic Ca^{2+} in $M\Phi_{BM}$ and $M\Phi_{TR}$, in line with the recently reported involvement of TRPV4 in stretch sensing in cardiac $M\Phi_{TR}$ (Wong,

Mohan et al., 2021), and in matrix stiffness sensing in skin MΦ (Dutta, Goswami & Rahaman 2020). TRP channels are not necessarily directly activated by stretch (Nikolaev, Cox et al., 2019), but may respond to stretch-induced activation of Piezo1, leading to cytosolic Ca^{2+} entry and increased open probability of Ca^{2+}-activated TRP channels (Yu, Gong et al., 2022). Such functional coupling, involving the several TRP channel subtypes, may underlie the large Ca^{2+} entry upon Yoda1 application in $M\Phi_{BM}$. Secondary channel activation via Piezo-induced Ca^{2+} entry has also been shown for Ca^{2+}-activated K^+-selective channels, such as the large-conductance BK channels (Jakob, Klesen et al., 2021), which is lowly expressed in the here studied MΦ populations (not shown). Data presented here and by others propose TRPV4 as a strong candidate to mediate mechano-immunity (Michalick & Kuebler 2020). Further experiments are needed to dissect the functional interactions of MSC with one-another, both in the plasma membrane and in intracellular membranes, to fully understand channel-based MΦ mechanosensation.

$M\Phi_{BM}$ may not represent a suitable model to study MSC activity in $M\Phi_{TR}$ and $M\Phi_{MD}$

While $M\Phi_{BM}$ provide a convenient model to study MΦ properties, the extent to which these cells reflect $M\Phi_{TR}$ and $M\Phi_{MD}$ mechanosensitivity is unknown. We find that, in contrast to $M\Phi_{BM}$, Piezo1 activity is minor in the plasma membrane of $M\Phi_{TR}$ isolated from healthy myocardium. This suggests that $M\Phi_{BM}$ may not be a suitable model system for the study of $M\Phi_{TR}$ mechanosensitivity.

As Piezo1 expression is upregulated in pathologically remodelled tissue exhibiting increased matrix stiffness (Chen, Wanggou et al., 2018; Jakob, Klesen et al., 2021; Li, Zhang et al., 2022), we explored whether Piezo1 activity in cardiac MΦ is altered in lesioned ventricular tissue. To this end, we compared stretch-induced currents and responses to Yoda1 application in murine MΦ, isolated from scar tissue and remote myocardium 3–4 weeks after ventricular cryoablation to those in control $M\Phi_{TR}$. Ventricular cryoinjury did not cause a significant increase in the percentage of cells responding to membrane stretch and did not result in significantly larger currents in the presence of Yoda1 even though the myocardium after ventricular injury is expected to contain both $M\Phi_{TR}$ and $M\Phi_{MD}$. scRNA-seq data show that *Piezo1* and *Trpv4* expression are significantly lower in $M\Phi_{MD}$ ($Ccr2^+$ MΦ) 28 days after surgery compared to $M\Phi_{TR}$ ($Timd4^+$ MΦ), while MΦ polarisation does not seem to significantly affect *Piezo1* expression. Indeed, using Ly6C as a marker (Epelman, Lavine et al., 2014), *Piezo1* expression was not significantly different between $Ly6C^{high}$ and $Ly6C^{low}$ MΦ (data not shown). Together, this suggests that $M\Phi_{BM}$ are not a suitable model system for the study of $M\Phi_{MD}$ mechanosensitivity either. Further research is needed to fully dissect the determinants and temporal dynamics of MSC expression and activity in the different MΦ populations during cardiac scar formation.

Taken together, these results suggest that the *in vitro*-derived $M\Phi_{BM}$ model is not suitable for characterisation of MSC activity in cardiac MΦ. In future studies, it would be interesting to selectively characterise the MSC activity profile of MΦ populations present at defined time points following myocardial injury.

In conclusion, this study confirms the presence of cation non-selective MSC in $M\Phi_{BM}$ and characterises them in $M\Phi_{TR}$. While Piezo1 mediates stretch-induced currents in $M\Phi_{BM}$, Piezo1 activity in the plasma membrane is minor in $M\Phi_{TR}$, where TRPV4 channels are prominent candidates to underlie MSC activity. Although MΦ populations in lesioned myocardium are expected to include cells derived from circulating monocytes, for which Piezo1 activity has been shown to be of functional importance (Forget, Gianni-Barrera et al., 2019), no increase in Piezo1 activity upon Yoda1 application was detected in cardiac MΦ post-cryoablation. This suggests either that $M\Phi_{MD}$, once recruited into cardiac tissue, undergo a phenotypic change in the direction of $M\Phi_{TR}$, or that the protocols we and others use to derive $M\Phi_{BM}$ from bone marrow (using 7-day-exposure to L929-cell conditioned medium) yields cells that differ from cardiac MΦ *in vivo*. Future experiments are needed to further characterise the molecular identity of channels underlying stretch-induced currents, and their functions in cardiac $M\Phi_{TR}$ and $M\Phi_{MD}$.

Supplementary results. Assessment of Piezo1 protein expression is challenged by unspecific antibody binding (Fig. **S2**)

Using a previously published (Vero Li et al., 2021; Zhou et al., 2021), commercially available antibody (P2-75617, Novus Biologicals), we assessed endogenous Piezo1 expression in $M\Phi_{BM}$ and $M\Phi_{TR}$ and exogenous Piezo1 expression (following transfection) in HEK cells by Western blot analysis (Supporting information, Fig. S2). The band corresponding to Piezo1 (286 kDa) can be detected in $M\Phi_{BM}$ when using 400,000 cells (red arrow, Fig. S2*A*), but not when using lower numbers of cells (Fig. S2*B*). No band for Piezo1 was detected when loading 30,000 $M\Phi_{TR}$ (number of cells isolated from one mouse heart). Overexpression of Piezo1 in HEK cells provided a strong signal using the same antibody. Notably, gels were characterised by bands of lower molecular mass, indicative of unspecific antibody binding. To explore intracellular localisation of Piezo1, we assessed whether the same antibody can be used for immunocytochemistry. In HAF with known Piezo1 expression at the plasma membrane,

strong fluorescence signals were observed in control cells and those after knock-down of Piezo1 expression by siRNA (Fig. S2*C*). Fluorescence intensity was not different between control cells and cells after knock-down (Fig. S2*D–E*), despite reduction of Piezo1 mRNA by >90%, as shown by qPCR (all experiments performed 72 h after transfection, Fig. S2*F*). Finally, we assessed Piezo1 staining in live $M\Phi_{BM}$ and $M\Phi_{TR}$ by flow cytometry. We detected Piezo1 surface expression in 98.5% ($N = 1$) and 79.5% ($N = 2$) of $M\Phi_{BM}$ and $M\Phi_{TR}$, respectively (Fig. S2*G* and *H*). Data interpretation remains difficult given the unspecific binding of the Piezo1 antibody observed in Western blot and immunocytochemistry data.

References

Afgan, E., Baker, D., Batut, B., Van Den Beek, M., Bouvier, D., Čech, M., Chilton, J., Clements, D., Coraor, N., Grüning, B. A., Guerler, A., Hillman-Jackson, J., Hiltemann, S., Jalili, V., Rasche, H., Soranzo, N., Goecks, J., Taylor, J., Nekrutenko, A., & Blankenberg, D. (2018). The Galaxy platform for accessible, reproducible and collaborative biomedical analyses: 2018 update. *Nucleic Acids Research*, **46**(W1), W537–W544.

Atcha, H., Jairaman, A., Holt, J. R., Meli, V. S., Nagalla, R. R., Veerasubramanian, P. K., Brumm, K. T., Lim, H. E., Othy, S., Cahalan, M. D., Pathak, M. M., & Liu, W. F. (2021). Mechanically activated ion channel Piezo1 modulates macrophage polarization and stiffness sensing. *Nature Communications*, **12**(1), 3256.

Bajpai, G., Schneider, C., Wong, N., Bredemeyer, A., Hulsmans, M., Nahrendorf, M., Epelman, S., Kreisel, D., Liu, Y., Itoh, A., Shankar, T. S., Selzman, C. H., Drakos, S. G., & Lavine, K. J. (2018). The human heart contains distinct macrophage subsets with divergent origins and functions. *Nature Medicine*, **24**(8), 1234–1245.

Baratchi, S., Zaldivia, M. T. K., Wallert, M., Loseff-Silver, J., Al-Aryahi, S., Zamani, J., Thurgood, P., Salim, A., Htun, N. M., Stub, D., Vahidi, P., Duffy, S. J., Walton, A., Nguyen, T. H. A., Jaworowski, A., Khoshmanesh, K., & Peter, K. (2020). Transcatheter aortic valve implantation represents an anti-inflammatory therapy via reduction of shear stress-induced, piezo-1-mediated monocyte activation. *Circulation*, **142**(11), 1092–1105.

Beaulieu-Laroche, L., Christin, M., Donoghue, A., Agosti, F., Yousefpour, N., Petitjean, H., Davidova, A., Stanton, C., Khan, U., Dietz, C., Faure, E., Fatima, T., Macpherson, A., Mouchbahani-Constance, S., Bisson, D. G., Haglund, L., Ouellet, J. A., Stone, L. S., Samson, J., Smith, M.-J. O., Ask, K., Ribeiro-Da-Silva, A., Blunck, R., Poole, K., Bourinet, E., & Sharif-Naeini, R. (2020). TACAN is an ion channel involved in sensing mechanical pain. *Cell*, **180**(5), 956–967. e17 e917.

Beech, D. J., & Kalli, A. C. (2019). Force sensing by piezo channels in cardiovascular health and disease. *Arteriosclerosis, Thrombosis, and Vascular Biology*, **39**(11), 2228–2239.

Chakarov, S., Lim, H. Y., Tan, L., Lim, S. Y., See, P., Lum, J., Zhang, X.-M., Foo, S., Nakamizo, S., Duan, K., Kong, W. T., Gentek, R., Balachander, A., Carbajo, D., Bleriot, C., Malleret, B., Tam, J. K. C., Baig, S., Shabeer, M., Toh, S.-A. E.e S., Schlitzer, A., Larbi, A., Marichal, T., Malissen, B., Chen, J., Poidinger, M., Kabashima, K., Bajenoff, M., Ng, L. G., Angeli, V., & Ginhoux, F. (2019). Two distinct interstitial macrophage populations coexist across tissues in specific subtissular niches. *Science*, **363**(6432), eaau0964.

Chen, X., Wanggou, S., Bodalia, A., Zhu, M., Dong, W., Fan, J. J., Yin, W. C., Min, H.-K., Hu, M., Draghici, D., Dou, W., Li, F., Coutinho, F. J., Whetstone, H., Kushida, M. M., Dirks, P. B., Song, Y., Hui, C.-C., Sun, Y. U., Wang, L. U.-Y., Li, X., & Huang, X. I. (2018). A feedforward mechanism mediated by mechanosensitive ion channel PIEZO1 and tissue mechanics promotes glioma aggression. *Neuron*, **100**(4), 799–815. e7.e797.

Delmas, P., Parpaite, T., & Coste, B. (2022). PIEZO channels and newcomers in the mammalian mechanosensitive ion channel family. *Neuron*, **110**(17), 2713–2727.

Dutta, B., Goswami, R., & Rahaman, S. O. (2020). TRPV4 plays a role in matrix stiffness-induced macrophage polarization. *Frontiers in Immunology*, **11**, 570195.

Emig, R., Zgierski-Johnston, C. M., Timmermann, V., Taberner, A. J., Nash, M. P., Kohl, P., & Peyronnet, R. (2021). Passive myocardial mechanical properties: Meaning, measurement, models. *Biophysical Reviews*, **13**(5), 587–610.

Epelman, S., Lavine, K. J., Beaudin, A. E., Sojka, D. K., Carrero, J. A., Calderon, B., Brija, T., Gautier, E. L., Ivanov, S., Satpathy, A. T., Schilling, J. D., Schwendener, R., Sergin, I., Razani, B., Forsberg, E. C., Yokoyama, W. M., Unanue, E. R., Colonna, M., Randolph, G. J., & Mann, D. L. (2014). Embryonic and adult-derived resident cardiac macrophages are maintained through distinct mechanisms at steady state and during inflammation. *Immunity*, **40**(1), 91–104.

Fernandez, M. C., Kopton, R. A., Simon-Chica, A., Madl, J., Hilgendorf, I., Zgierski-Johnston, C. M., & Schneider-Warme, F. (2021). Channelrhodopsins for cell-type specific illumination of cardiac electrophysiology. *Methods in Molecular Biology*, **2191**, 287–307.

Forget, A., Gianni-Barrera, R., Uccelli, A., Sarem, M., Kohler, E., Fogli, B., Muraro, M. G., Bichet, S., Aumann, K., Banfi, A., & Shastri, V. P. (2019). Mechanically defined microenvironment promotes stabilization of microvasculature, which correlates with the enrichment of a novel piezo-1^+ population of circulating $CD11b^+/CD115^+$ monocytes. *Advanced Materials*, **31**(21), e1808050.

Gannier, F., White, E., Lacampagne, A., Garnier, D., & Guennec, J.-Y. L. (1994). Streptomycin reverses a large stretch induced increase in $[Ca^{2+}]_i$ in isolated guinea pig ventricular myocytes. *Cardiovascular Research*, **28**(8), 1193–1198.

Greiner, J., Schiatti, T., Kaltenbacher, W., Dente, M., Semenjakin, A., Kok, T., Fiegle, D. J., Seidel, T., Ravens, U., Kohl, P., Peyronnet, R., & Rog-Zielinska, E. A. (2022). Consecutive-day ventricular and atrial cardiomyocyte isolations from the same heart: Shifting the cost-benefit balance of cardiac primary cell research. *Cells*, **11**(2), 233.

Heidt, T., Courties, G., Dutta, P., Sager, H. B., Sebas, M., Iwamoto, Y., Sun, Y., Da Silva, N., Panizzi, P., Van Der Laan, A. M., Swirski, F. K., Weissleder, R., & Nahrendorf, M. (2014). Differential contribution of monocytes to heart macrophages in steady-state and after myocardial infarction. *Circulation Research*, **115**(2), 284–295.

Hulsmans, M., Clauss, S., Xiao, L., Aguirre, A. D., King, K. R., Hanley, A., Hucker, W. J., Wülfers, E. M., Seemann, G., Courties, G., Iwamoto, Y., Sun, Y., Savol, A. J., Sager, H. B., Lavine, K. J., Fishbein, G. A., Capen, D. E., Da Silva, N., Miquerol, L., Wakimoto, H., Seidman, C. E., Seidman, J. G., Sadreyev, R. I., Naxerova, K., Mitchell, R. N., Brown, D., Libby, P., Weissleder, R., Swirski, F. K., Kohl, P., Vinegoni, C., Milan, D. J., Ellinor, P. T., & Nahrendorf, M. (2017). Macrophages facilitate electrical conduction in the heart. *Cell*, **169**(3), 510–522. e20.

Jakob, D., Klesen, A., Allegrini, B., Darkow, E., Aria, D., Emig, R., Chica, A. S., Rog-Zielinska, E. A., Guth, T., Beyersdorf, F., Kari, F. A., Proksch, S., Hatem, S. N., Karck, M., Künzel, S. R., Guizouarn, H., Schmidt, C., Kohl, P., Ravens, U., & Peyronnet, R. (2021). Piezo1 and BK(Ca) channels in human atrial fibroblasts: Interplay and remodelling in atrial fibrillation. *Journal of Molecular and Cellular Cardiology*, **158**, 49–62.

Jiang, F., Yin, K., Wu, K., Zhang, M., Wang, S., Cheng, H., Zhou, Z., & Xiao, B. (2021). The mechanosensitive Piezo1 channel mediates heart mechano-chemo transduction. *Nature Communications*, **12**(1), 869.

Künzel, S. R., Rausch, J. S. E., Schäffer, C., Hoffmann, M., Künzel, K., Klapproth, E., Kant, T., Herzog, N., Küpper, J.-H., Lorenz, K., Dudek, S., Emig, R., Ravens, U., Rog-Zielinska, E. A., Peyronnet, R., & El-Armouche, A. (2020). Modeling atrial fibrosis in vitro-Generation and characterization of a novel human atrial fibroblast cell line. *FEBS Open Biology*, **10**(7), 1210–1218.

Lee, M., Du, H., Winer, D. A., Clemente-Casares, X., & Tsai, S. (2022). Mechanosensing in macrophages and dendritic cells in steady-state and disease. *Frontiers in Cell and Developmental Biology*, **10**, 1044729.

Li, M., Zhang, X.i, Wang, M., Wang, Y., Qian, J., Xing, X., Wang, Z., You, Y., Guo, K., Chen, J., Gao, D., Zhao, Y., Zhang, L., Chen, R., Cui, J., & Ren, Z. (2022). Activation of Piezo1 contributes to matrix stiffness-induced angiogenesis in hepatocellular carcinoma. *Cancer Communications*, **42**(11), 1162–1184.

Liao, J., Lu, W., Chen, Y., Duan, X., Zhang, C., Luo, X., Lin, Z., Chen, J., Liu, S., Yan, H., Chen, Y., Feng, H., Zhou, D., Chen, X.u, Zhang, Z., Yang, Q., Liu, X., Tang, H., Li, J., Makino, A., Yuan, J. X.-J., Zhong, N., Yang, K., & Wang, J. (2021). Upregulation of piezo1 (piezo type mechanosensitive ion channel component 1) enhances the intracellular free calcium in pulmonary arterial smooth muscle cells from idiopathic pulmonary arterial hypertension patients. *Hypertension*, **77**(6), 1974–1989.

Liao, Y., Smyth, G. K., & Shi, W. (2014). featureCounts: An efficient general purpose program for assigning sequence reads to genomic features. *Bioinformatics*, **30**(7), 923–930.

Liu, H., Hu, J., Zheng, Q., Feng, X., Zhan, F., Wang, X., Xu, G., & Hua, F. (2022). Piezo1 channels as force sensors in mechanical force-related chronic inflammation. *Frontiers in Immunology*, **13**, 816149.

Lother, A., Bondareva, O., Saadatmand, A. R., Pollmeier, L., Härdtner, C., Hilgendorf, I., Weichenhan, D., Eckstein, V., Plass, C., Bode, C., Backs, J., Hein, L., & Gilsbach, R. (2021). Diabetes changes gene expression but not DNA methylation in cardiac cells. *Journal of Molecular and Cellular Cardiology*, **151**, 74–87.

Mchugh, B. J., Buttery, R., Lad, Y., Banks, S., Haslett, C., & Sethi, T. (2010). Integrin activation by Fam38A uses a novel mechanism of R-Ras targeting to the endoplasmic reticulum. *Journal of Cell Science*, **123**(Pt 1), 51–61.

Michalick, L., & Kuebler, W. M. (2020). TRPV4-A missing link between mechanosensation and immunity. *Frontiers in Immunology*, **11**, 413.

Nicolás-Ávila, J. A., Lechuga-Vieco, A. V., Esteban-Martínez, L., Sánchez-Díaz, M., Díaz-García, E., Santiago, D. J., Rubio-Ponce, A., Li, J. L., Balachander, A., Quintana, J. A., Martínez-De-Mena, R., Castejón-Vega, B., Pun-García, A., Través, P. G., Bonzón-Kulichenko, E., García-Marqués, F., Cussó, L., A-González, N., González-Guerra, A., … Hidalgo, A. (2020). A network of macrophages supports mitochondrial homeostasis in the heart. *Cell*, **183**(1), 94–109. e23.

Nikolaev, Y. A., Cox, C. D., Ridone, P., Rohde, P. R., Cordero-Morales, J. F., Vasquez, V., Laver, D. R., & Martinac, B. (2019). Mammalian TRP ion channels are insensitive to membrane stretch. *Journal of Cell Science*, **132**(23), jcs238360.

Pachitariu, M., & Stringer, C. (2022). Cellpose 2.0: How to train your own model. *Nature Methods*, **19**(12), 1634–1641.

Parkhurst, C. N., Yang, G., Ninan, I., Savas, J. N., Yates, J. R., Lafaille, J. J., Hempstead, B. L., Littman, D. R., & Gan, W.-B. (2013). Microglia promote learning-dependent synapse formation through BDNF. *Cell*, **155**, 1596–1609.

Peyronnet, R., Nerbonne, J. M., & Kohl, P. (2016). Cardiac mechano-gated ion channels and arrhythmias. *Circulation Research*, **118**(2), 311–329.

Romani, P., Valcarcel-Jimenez, L., Frezza, C., & Dupont, S. (2021). Crosstalk between mechanotransduction and metabolism. *Nature Reviews Molecular Cell Biology*, **22**(1), 22–38.

Rosales-Alvarez, R. E., Rettkowski, J., Herman, J. S., Dumbović, G., Cabezas-Wallscheid, N., & Grün, D. (2023). VarID2 quantifies gene expression noise dynamics and unveils functional heterogeneity of ageing hematopoietic stem cells. *Genome Biology*, **24**(1), 148.

Santoni, G., Morelli, M. B., Amantini, C., Santoni, M., Nabissi, M., Marinelli, O., & Santoni, A. (2018). "Immuno-transient receptor potential ion channels": The role in monocyte- and macrophage-mediated inflammatory responses. *Frontiers in Immunology*, **9**, 1273.

Scheraga, R. G., Abraham, S., Niese, K. A., Southern, B. D., Grove, L. M., Hite, R. D., Mcdonald, C., Hamilton, T. A., & Olman, M. A. (2016). TRPV4 mechanosensitive ion channel regulates lipopolysaccharide-stimulated macrophage phagocytosis. *Journal of Immunology*, **196**(1), 428–436.

Schmidt, U., Weigert, M., Broaddus, C., & Myers, G. (2018). Cell detection with star-convex polygons. Medical Image Computing and Computer Assisted Intervention–MICCAI 2018: 21st International Conference, Granada, Spain, September 16–20, 2018, Proceedings, Part II 11, Springer.

Selezneva, A., Gibb, A. J., & Willis, D. (2022). The contribution of ion channels to shaping macrophage behaviour. *Frontiers in Pharmacology*, **13**, 970234.

Simon-Chica, A., Fernández, M. C., Wülfers, E. M., Lother, A., Hilgendorf, I., Seemann, G., Ravens, U., Kohl, P., & Schneider-Warme, F. (2022). Novel insights into the electrophysiology of murine cardiac macrophages: Relevance of voltage-gated potassium channels. *Cardiovascular Research*, **118**(3), 798–813.

Solis, A. G., Bielecki, P., Steach, H. R., Sharma, L., Harman, C. C. D., Yun, S., De Zoete, M. R., Warnock, J. N., To, S. D. F., York, A. G., Mack, M., Schwartz, M. A., Dela Cruz, C. S., Palm, N. W., Jackson, R., & Flavell, R. A. (2019). Mechanosensation of cyclical force by PIEZO1 is essential for innate immunity. *Nature*, **573**(7772), 69–74.

Stringer, C., Wang, T., Michaelos, M., & Pachitariu, M. (2021). Cellpose: A generalist algorithm for cellular segmentation. *Nature Methods*, **18**(1), 100–106.

Suchyna, T. M., Markin, V. S., & Sachs, F. (2009). Biophysics and structure of the patch and the gigaseal. *Biophysical Journal*, **97**(3), 738–747.

Syeda, R., Xu, J., Dubin, A. E., Coste, B., Mathur, J., Huynh, T., Matzen, J., Lao, J., Tully, D. C., Engels, I. H., Petrassi, H. M., Schumacher, A. M., Montal, M., Bandell, M., & Patapoutian, A. (2015). Chemical activation of the mechanotransduction channel Piezo1. *Elife*, **4**, e07369.

Tang, Y. U., Zhao, C., Zhuang, Y., Zhong, A., Wang, M., Zhang, W., & Zhu, L. (2023). Mechanosensitive Piezo1 protein as a novel regulator in macrophages and macrophage-mediated inflammatory diseases. *Frontiers in Immunology*, **14**, 1149336.

Vero Li, J., Cox, D. C., & Martinac, B. (2021). The anchor domain is critical for Piezo1 channel mechanosensitivity. *Channels (Austin)*. **15**(1), 438–446.

Vicente, R., Escalada, A., Coma, M., Fuster, G., Sánchez-Tilló, E., López-Iglesias, C., Soler, C., Solsona, C., Celada, A., & Felipe, A. (2003). Differential voltage-dependent K^+ channel responses during proliferation and activation in macrophages. *Journal of Biological Chemistry*, **278**(47), 46307–46320.

Villalonga, N., David, M., Bielanska, J., Vicente, R., Comes, N., Valenzuela, C., & Felipe, A. (2010). Immunomodulation of voltage-dependent K^+ channels in macrophages: Molecular and biophysical consequences. *Journal of General Physiology*, **135**(2), 135–147.

Weischenfeldt, J., & Porse, B. (2008). Bone marrow-derived macrophages (BMM): Isolation and applications. CSH Protoc. https://doi.org/10.1101/pdb.prot5080

Wong, N. R., Mohan, J., Kopecky, B. J., Guo, S., Du, L., Leid, J., Feng, G., Lokshina, I., Dmytrenko, O., Luehmann, H., Bajpai, G., Ewald, L., Bell, L., Patel, N., Bredemeyer, A., Weinheimer, C. J., Nigro, J. M., Kovacs, A., Morimoto, S., Bayguinov, P. O., Fisher, M. R., Stump, W. T., Greenberg, M., Fitzpatrick, J. A. J., Epelman, S., Kreisel, D., Sah, R., Liu, Y., Hu, H., & Lavine, K. J. (2021). Resident cardiac macrophages mediate adaptive myocardial remodeling. *Immunity*, **54**(9), 2072–2088. e7.

Xu, J., Gao, C., He, Y., Fang, X., Sun, D., Peng, Z., Xiao, H., Sun, M., Zhang, P., Zhou, T., Yang, X., Yu, Y., Li, R., Zou, X., Shu, H., Qiu, Y., Zhou, X.i, Yuan, S., Yao, S., & Shang, Y. (2023). NLRC3 expression in macrophage impairs glycolysis and host immune defense by modulating the NF-kappaB-NFAT5 complex during septic immunosuppression. *Molecular Therapy*, **31**(1), 154–173.

Yu, Z. E.-Y., Gong, H., Kesteven, S., Guo, Y., Wu, J., Li, J. V., Cheng, D., Zhou, Z., Iismaa, S. E., Kaidonis, X., Graham, R. M., Cox, C. D., Feneley, M. P., & Martinac, B. (2022). Piezo1 is the cardiac mechanosensor that initiates the cardiomyocyte hypertrophic response to pressure overload in adult mice. *Nature Cardiovascular Research*, **1**(6), 577–591.

Zhou, Z., Li, J. V., Martinac, B., & Cox, C. D. (2021). Loss-of-function piezo1 mutations display altered stability driven by ubiquitination and proteasomal degradation. *Frontiers in Pharmacology*, **12**, 766416.

Additional information

Data availability statement

The data generated or analysed during the present study are available from the corresponding author upon reasonable request.

Competing interests

The authors state that they have no conflict of interest.

Author contributions

S.-C.A., data curation, formal analysis, validation, investigation, visualisation, methodology, writing the original draft; K.A., E.R., C.A. and G.J., data curation, formal analysis, investigation, visualisation, methodology; G.D., L.A., H.I., R.-Z. E.A., R.U. and K.P., supervision, methodology, validation, resources; S.-W.F., conceptualisation, supervision, methodology, validation, ressources; R.P., conceptualisation, data curation, validation, visualisation, methodology, supervision and writing the original draft. All authors have read and approved the final version of this manuscript and agree to be accountable for all aspects of the work in ensuring that questions related to the accuracy or integrity of any part of the work are appropriately investigated and resolved. All persons designated as authors qualify for authorship, and all those who qualify for authorship are listed.

Funding

This study was supported by the German Research Foundation (DFG)-funded Collaborative Research Centre CRC1425 (DFG ID no. 422681845). The project received additional financial support via the Emmy-Noether programme (DFG ID no.

412853334 to F.S.W.) and via a 'la Caixa' Foundation PhD fellowship to S.-C.A. (ID no. 100010434). K.A. is supported by the Berta-Ottenstein-Programme for Clinician Scientists by the Faculty of Medicine, University of Freiburg. E.R. is supported by a post-doctoral fellowship from the German Cardiac Society (DGK).

Acknowledgements

The authors thank Stefanie Perez for performing the surgical interventions and Tomas Brennan for isolation of cells for single-cell sequencing. The authors thank all members of the Institute for Experimental Cardiovascular Medicine (IEKM) for critical discussion and input on the manuscript. The authors acknowledge the microscopy facility SCI-MED (Super-Resolution Confocal/Multiphoton Imaging for Multiparametric Experimental Designs) at IEKM, Freiburg, for providing access to imaging setups and analysis work stations, and its director, Josef Madl, for expert technical support. The authors thank the Lighthouse Facility of the University of Freiburg for providing access and support for cell sorting. All authors are members of the German Research Foundation (DFG)-funded Collaborative Research Centre CRC1425 (DFG ID no. 422681845).

Open access funding enabled and organized by Projekt DEAL.

Keywords

cryoablation, immunity, mechanotransduction, scar, TRPV4

Supporting information

Additional supporting information can be found online in the Supporting Information section at the end of the HTML view of the article. Supporting information files available:

Peer Review History
Figure S1
Figure S2